Tectonics

RESEARCH ARTICLE
10.1029/2022TC007679

Key Points:

- We build a balanced cross section across the Circeo thin-skinned thrust, one of the innermost structures of the central Apennines
- The section is validated by means of carbonate C and O and clumped isotopes, U-Pb dating, seismic interpretation and burial modeling
- A regional synthesis of the age of foredeep infill, thrusts, and extensional basins for the central Apennines is presented

Supporting Information:

Supporting Information may be found in the online version of this article.

Correspondence to:

S. Tavani,
stefano.tavani@unina.it

Citation:

Tavani, S., Smeraglia, L., Fabbi, S., Aldega, L., Sabbatino, M., Cardello, G. L., et al. (2023). Timing, thrusting mode, and negative inversion along the Circeo thrust, Apennines, Italy: How the accretion-to-extension transition operated during slab rollback. *Tectonics*, *42*, e2022TC007679. https://doi.org/10.1029/2022TC007679

Received 13 NOV 2022
Accepted 5 JUN 2023

Timing, Thrusting Mode, and Negative Inversion Along the Circeo Thrust, Apennines, Italy: How the Accretion-To-Extension Transition Operated During Slab Rollback

S. Tavani[1,2], L. Smeraglia[2], S. Fabbi[3], L. Aldega[3], M. Sabbatino[4], G. L. Cardello[5], A. Maresca[1], G. Schirripa Spagnolo[3], A. Kylander-Clark[6], A. Billi[2], S. M. Bernasconi[7], and E. Carminati[3]

[1]Università degli Studi di Napoli Federico II, Napoli, Italy, [2]Consiglio Nazionale delle Ricerche, IGAG, Roma, Italy, [3]Dipartimento di Scienze della Terra, Sapienza Università di Roma, Roma, Italy, [4]Department of Mathematics and Geosciences, University of Trieste, Trieste, Italy, [5]Dipartimento di Scienze Chimiche, Matematiche, Fisiche e Naturali, Università degli Studi di Sassari, Sassari, Italy, [6]Department of Earth Science, University of California, Santa Barbara, CA, USA, [7]Geological Institute, ETH Zürich, Zürich, Switzerland

Abstract The evolution of the Apennine wedge has seen the time-space migration of the forebulge, foredeep, thrust wedge, and back-arc extension phases in the wake of the Eastward rollback of the subducting Adria slab. In this framework, thrusting and post-orogenic extensional faulting have occurred in two parallel forelandward-migrating ribbons, with extensional deformation overprinting or partly exploiting anisotropies of the inherited thrust system. Here, we explore the tectonic framework and the timing of thrusting and subsequent negative inversion of the Circeo thrust, one of the major thrusts in the inner portion of the central Apennines, with the main aim to constrain the timing and mode of the compression to extension switch. Structural analysis, carbonate C and O and clumped isotopes analysis, X-ray diffraction of clay minerals, and U-Pb dating of calcite slickenfibers have been integrated with seismic interpretation, cross-section balancing, and 1D burial and thermal modeling. We show that the Circeo thrust developed during Langhian-Serravallian time. Its extensional reactivation is dated at the Serravallian, during the stacking of an underlying thrust slice, before the onset of Pliocene back-arc extension in the area. Combination of our data with the age of thrusts, extensional basins, and base of the foredeep infill of the central Apennines, demonstrates that forelandward migration of the foredeep-thrust system occurred at variable velocities. Accelerations and decelerations are synchronous, respectively, with the opening of the Liguro-Provençal and Tyrrhenian back-arc basins and with the interluding quiescent period.

1. Introduction

Negative inversion and extensional reactivation of pre-existing compressive structures can occur at temporal scales ranging from seconds to millions of years. It may relate to multiple processes (e.g., Tari et al., 2023), spanning from local post-seismic stress reorganization (e.g., Hardebeck & Okada, 2018; Meneghini & Moore, 2007) up to the plate scale of the Wilson cycle, with opening of rift basins favored by the reactivation of inherited compressive structures (Wilson, 1966). In the actively deforming Apennine belt of Italy, the Eastward retreat of the subduction zone since the Oligocene led to thrusting and wedge accretion followed by crustal stretching associated with back-arc basins (e.g., Carminati et al., 2012; Doglioni, 1991; Faccenna et al., 2004, 2014) (Figure 1a), whose delay and interplay is still matter of debate. Moreover, the geodynamic significance of extensional structures is debated. According to some authors, many extensional faults developed at shallow crustal levels before back-arc extension, due to gravitational re-equilibration of the upper portion of antiformal stacks during thrusting (e.g., Ghisetti & Vezzani, 2000; Storti et al., 2018; Tavani et al., 2012). The documented negative inversion of thrusts suggests their key role in the localization of deformation during extension (e.g., Curzi, Aldega, et al., 2020; D'Agostino et al., 1998; Pace et al., 2017). Indeed, these compressional structures could have favored the inception of extensional deformation way before the main crustal stretching phase and thus they could now help in unveiling the switch from compression to extension. Understanding the timing and mode of this switch is of primary interest in an actively deforming area such as the Apennines (e.g., Montone & Mariucci, 2016), where $M_w > 6$ compressive and extensional earthquakes occur in the outer and inner portion of the belt, respectively (e.g., Chiarabba et al., 2005;

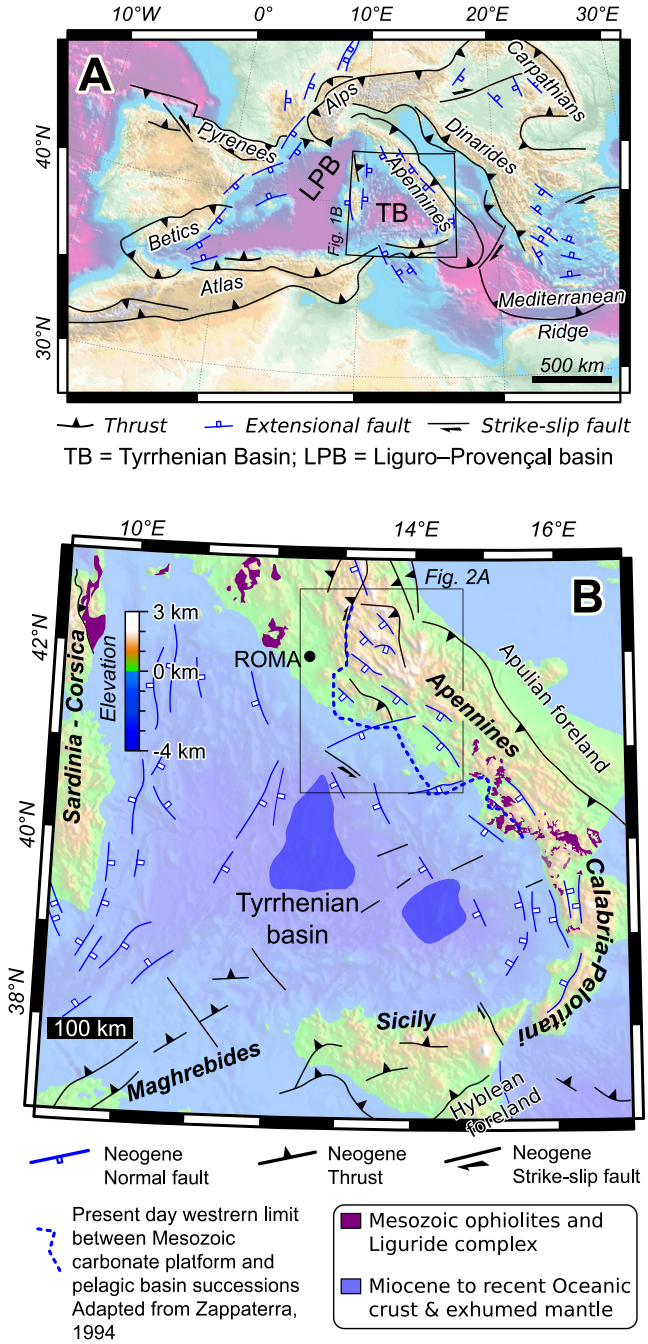

Figure 1. Structural schemes of: (a) the western Mediterranean area and (b) Tyrrhenian basin and central Apennines, with Miocene to Quaternary oceanic crust and exhumed mantle in the Tyrrhenian abyssal plain, and Mesozoic Tethyan ophiolites (Liguride complex) indicated.

Rovida et al., 2020). Direct observations of negative inversion in the inner portions of the belt, where thrust systems are exposed, provide an opportunity to study tectonic processes that in the more external portions of the belt, where seismicity is currently active, occur at deeper structural levels and cannot be directly observed. In these internal areas, the fingerprint of fault reactivation in dilatant/extensional regime includes the following diagnostic features along the inverted fault zones: superimposed S-C/C′ fabrics with opposite kinematics (e.g., Curzi, Aldega, et al., 2020), dilatation and mineral infilling of S surfaces and pressure-solution seams (e.g., Meneghini & Moore, 2007), and folding of S-C/C′ fabric with an overall opposite shear sense (e.g., Tavani et al., 2011). Multiple techniques, such as X-ray diffraction (XRD) of clay minerals (mixed layer illite-smectite, Aldega et al., 2021) optical analysis of the organic matter (vitrinite reflectance, Balestra et al., 2019), Raman spectroscopy of carbonaceous materials (Beyssac et al., 2002; Schito et al., 2017), low-temperature thermochronology (e.g., Ault et al., 2019; Fellin et al., 2022), calcite twinning paleopiezometry (e.g., Lacombe et al., 2007) and stylolite roughness (e.g., Labeur et al., 2021) can be applied to constrain stress and maximum burial conditions during thrusting and inversion. Similarly, geochemical analyses (e.g., C and O isotopes) can be carried out on mineralizations hosted along fault zones (Smeraglia et al., 2019; Uysal et al., 2006) and in the surrounding areas (e.g., Evans & Fischer, 2012), to investigate fault-fluid interactions (e.g., Lucca et al., 2019), and decipher exhumation, burial, and changes in the structural style of deformation (e.g., Beaudoin et al., 2014; Cruset et al., 2018). The potential of these techniques and data increases when combined with radiometric dating (e.g., Cruset et al., 2020; Curzi, Aldega, et al., 2020; Lacombe & Beaudoin, 2024; Lacombe et al., 2021; Wang et al., 2016) and when all the above observations or part of them are implemented into balanced cross sections and structural models (e.g., Beaudoin et al., 2012; Ducoux et al., 2021; McQuarrie et al., 2008).

The aim of this study is to constrain the time and mode of switch between thrusting and extension for the Circeo thrust, the innermost exposed thrust of the central Apennines that shows evidence of slip reversal, by integrating seismic and field data with 1D burial and thermal models constrained by original mixed layer illite-smectite data, and previously published apatite fission track and U-Th/He dating. In addition, we used structural and microstructural observations along the thrust zone and carbonate C, O, and clumped isotopes analysis and U-Pb dating of calcite slickenfibers to characterize their age and formation temperatures. We present a balanced cross-section that illuminates the framework of thrusting and subsequent negative inversion. The regional implications of our findings in the framework of the central Apennine's thrust belt evolution are highlighted. In particular, our data provide crucial time constraints on early thrusting in the central Apennines, of which little is known. Furthermore, they allow us to link the small-sized and unevenly distributed exposures of syn-orogenic deposits of the Tyrrhenian margin of the belt. Eventually, our data set is integrated into existing data on the age of compressional and extensional structures across the entire central Apennines. Specifically, by comparing the variations in the rate of foredeep/forebulge and thrust system migration across the central Apennine belt with phases of back-arc extension, we speculate about the larger scale dynamics of thrust wedge advance and slab rollback velocities. We propose that this study may be used as a reference example to understand the evolution of fold-thrust belts and the post-orogenic extension in relation to the velocities of the retreat of subducting slabs.

2. Geological Setting

2.1. The Apennine-Tyrrhenian Basin System

The Apennines, the Calabria-Peloritani Arc, and the Sicilian-Maghrebian chain form an orocline cored by the Tyrrhenian back-arc basin (Figure 1). The development of this orocline is associated with the ESE-ward retreating subduction of the Alpine Tethys and of its southern passive margin (Adria) underneath Europe (i.e., the northern margin of the Alpine Tethys) (e.g., Carminati & Doglioni, 2012; Doglioni, 1991; Faccenna et al., 2004; Molli, 2008). The Apennines are characterized by a dominantly thin-skinned tectonic style (e.g., Ghisetti et al., 1993; Mostardini & Merlini, 1986; Tavani, Granado, et al., 2021), with a main detachment in the Triassic siliciclastic redbeds of the Verrucano group and underlying metasediments (e.g., Mirabella et al., 2008; Patacca et al., 2008; Volpe et al., 2022), which unconformably overlie the Variscan crystalline basement (e.g., Cassinis et al., 2018). Limited involvement of the Variscan crystalline basement of the lower plate is only documented for the final stage of convergence (e.g., Billi et al., 2006; Tavani, Granado, et al., 2021). Thin-skinned thrusting and nappe stacking has progressed from west to east (e.g., Barchi, 2010; Cavinato & De Celles, 1999; Menardi Noguera & Rea, 2000; Sabbatino et al., 2021). Thrusting involved first the sedimentary cover of the Tethys Ocean and slices of ophiolites (Liguride complex) scraped off from the down-going Tethys oceanic plate (Knott, 1987; Marroni et al., 1998) and since the Late Oligocene, the sedimentary successions of the Adria passive margin. These successions were deposited during Late Triassic to Early Jurassic rifting and the subsequent opening of the Alpine Tethys Ocean (e.g., Menardi Noguera & Rea, 2000; Santantonio & Carminati, 2011; Zappaterra, 1994) and were followed by late Cenozoic syn-orogenic foredeep sediments. Slab rollback and eastward retreat of the trench led to extensional deformation and volcanism at the rear of the compressive front (e.g., Cavinato & De Celles, 1999; Doglioni, 1991; Faccenna et al., 2004; Jolivet et al., 2009; Storti, 1995). Crustal stretching led to the opening of the Late Oligocene-Burdigalian Liguro–Provençal back-arc basin (e.g., Gattacceca et al., 2007) and of the Serravallian/Tortonian to present-day Tyrrhenian back-arc basin (e.g., Jolivet et al., 1998; Mattei et al., 2002; Sartori et al., 2001, Figure 1). The central portion of the Tyrrhenian back-arc basin is floored by exhumed subcontinental mantle and Messinian to Pleistocene oceanic crust (e.g., Jolivet et al., 2021; Kastens & Mascle, 1990; Sartori et al., 2004; Savelli & Ligi, 2017). The Apenninic margin of the Tyrrhenian basin is instead affected by mostly <1 Ma to Present potassic to ultra-potassic volcanism developed coevally with extensional tectonics (e.g., Acocella & Funiciello, 2006; Carminati et al., 2012).

2.2. The Central Apennines

The sedimentary succession of the central Apennines mostly belongs to the Mesozoic Latium-Abruzzi carbonate platform and the surrounding pelagic basins, which developed on the Adria passive margin after the Triassic to Early Jurassic rifting (e.g., Bernoulli et al., 1979; Zappaterra, 1994). Early Jurassic syn-rift faults in the central and northern Apennines are nowadays N-S and E-W striking (Castellarin et al., 1978; Fabbi, 2015; Pierantoni et al., 2013; Storti et al., 2018) and developed horst and graben structures on which, in first approximation, carbonate platform and pelagic basin sedimentation has been established. The Circeo pelagic basin, whose remnants are exposed in the Circeo promontory, was bound to the north by the Latium-Abruzzi carbonate platform. Parts of the Circeo basinal and slope succession were drilled in the Mara-1, Michela-1, Fogliano-1, and Tre Cancelli deep wells (Figures 2a and 2b). Moreover, they occur as exotic blocks within the Upper Miocene-Pliocene chaotic complex of the Volsci Range and as clasts in the Upper Miocene Villa Treglia conglomerate exposed in the Formia plain, 50 km to the east of the Circeo promontory (Tavani, Cardello, et al., 2021).

The central Apennines are composed of NW-SE oriented thrust sheets affected by NW-SE striking post-thrusting extensional faults (e.g., Cavinato & De Celles, 1999; Cosentino et al., 2010; Patacca et al., 2008). From the internal (SW) to the external (NE) portion of the belt, the main thrust sheets are (Figure 2a): the Zannone Island, the Circeo promontory, the Volsci Range, the Simbruini-Ernici Range, the Marsica thrust sheet, and the Gran Sasso Range. Along the Tyrrhenian margin, between the Volsci Range and the Circeo promontory (Figure 2a), another buried major thrust (Mara thrust), connects, in our view, the thrust zone found in the Mara-1 well (Figure 2b) with the lower thrust of the Circeo promontory documented in this work. The W-dipping Olevano-Antrodoco thrust formed as an out-of-sequence oblique structure reactivating an inherited N-S striking Early Jurassic extensional fault (e.g., Castellarin et al., 1978). In the Zannone Island, K-Ar dating of the major thrust yielded an Aquitanian age (22.1 ± 0.6 Ma; Curzi, Billi, et al., 2020); in the Mt. Massico area, the south-eastern continuation of the Volsci Range thrust (Smeraglia et al., 2019), U-Pb dating of calcite slickenfibers on thrusts and normal faults indicates

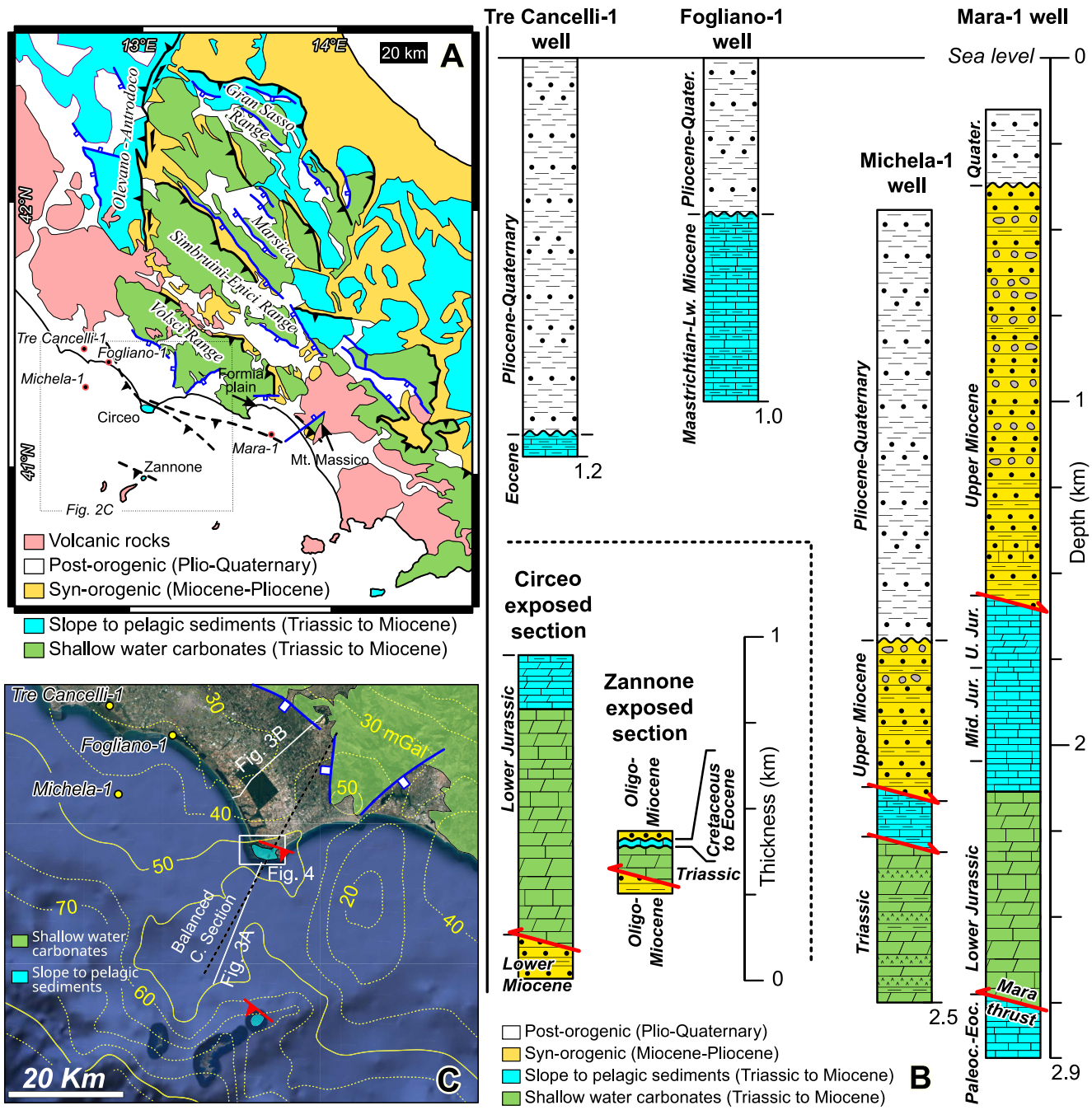

Figure 2. (a) Geological map of the central Apennines. (b) Stratigraphy of the deep wells of the broad study area and simplified stratigraphic sequences of the Zannone (excluding the upper Pliocene-Pleistocene volcanics) and Circeo thrust areas. (c) Simplified geological scheme of the Circeo area, with Bouguer anomalies (https://www.isprambiente.gov.it/it), and traces of seismic lines of Figure 3 and balanced cross section of Figure 12.

that thrusting is Messinian to Pliocene in age (7.0 ± 1.6 and 5.1 ± 3.7 Ma) and it is postdated by Late Pliocene to earliest Pleistocene extension (2.85 ± 0.5 Ma; Smeraglia et al., 2019). Coherently, stratigraphic criteria point to a Tortonian/Messinian to Pliocene interval for the Volsci Range thrust sheet development (Cardello et al., 2021) and Messinian to Pliocene compression in the Formia Plain in the footwall of the Mara thrust, followed by Pleistocene extension (Tavani, Cardello, et al., 2021). Finally, single-grain apatite U-Th/He (AHe) age from the flysch in the footwall of the Circeo thrust indicates exhumation and cooling to ~60° at 5.8 ± 0.9 Ma (Fellin et al., 2022).

Syn-orogenic deposits cropping out in the onshore central Apennines and drilled in the Adriatic foredeep have been extensively studied (e.g., Cipollari & Cosentino, 1995), and the time-transgressive base of the foredeep

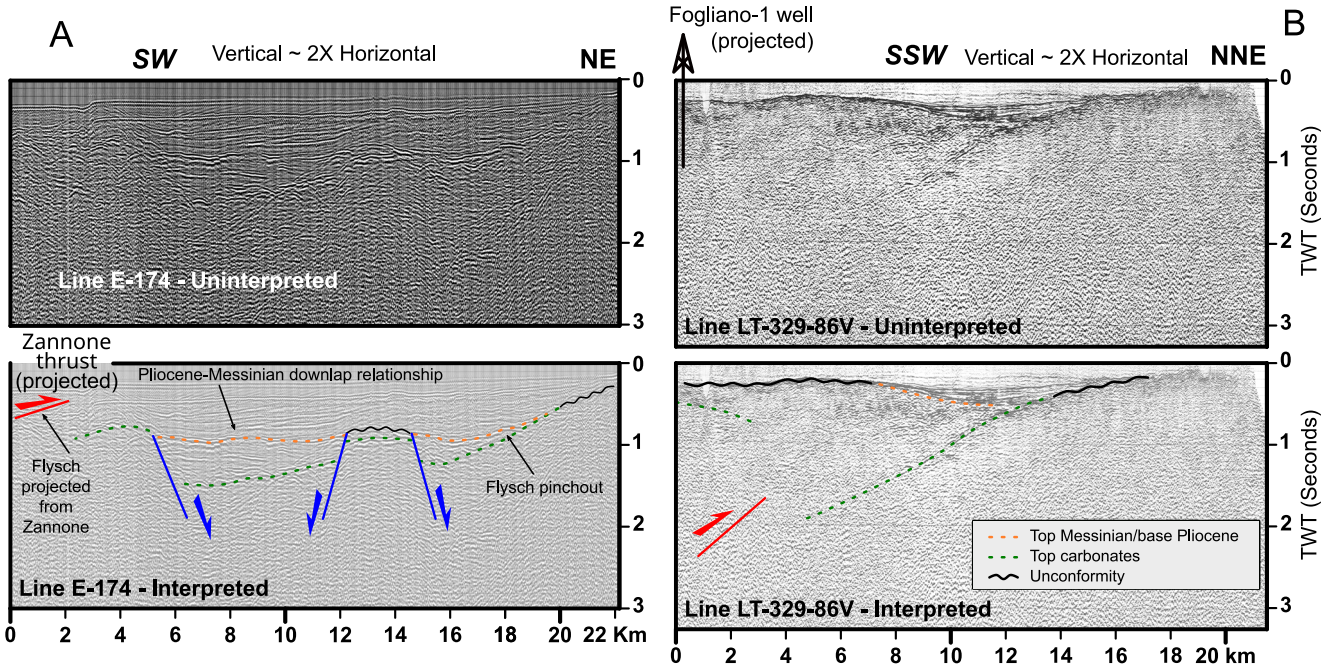

Figure 3. Interpreted and uninterpreted seismic lines (traces of the lines are in Figure 2). The Fogliano 1 well and the Zannone exposure are projected using the NW-SE trend of the Apenninic structures.

infill clearly gets younger toward the foreland (Sabbatino et al., 2021). Instead, little is known about the internal syn-orogenic deposits that are unevenly exposed along the Tyrrhenian margin of the central Apennines. For example, the Upper Miocene flysch unit exposed between the Formia plain and the Mt. Massico area is interfingered with an enigmatic fan delta conglomerate that includes mostly clasts of deep-water carbonates, but also of granite (Tavani, Cardello, et al., 2021). Analogously, the age of the lower Miocene flysch unit exposed at the Circeo promontory has a large degree of uncertainty (Accordi, 1966) and the small size of this exposure does not allow to infer its depositional setting. An even larger uncertainty affects the age attribution of the siliciclastic deposit in the footwall of the Zannone thrust. This deposit, previously believed to be a Permian unit, has been interpreted as a Cenozoic flysch only in very recent times (Curzi, Billi, et al., 2020).

2.3. The Circeo Promontory

The Circeo promontory forms an about 0.5 km high, 5 km long, and 3 km wide ridge (Figure 2c), surrounded by Pliocene-Quaternary coastal sediments. The backbone of the promontory is made up of N-dipping pre-rift shallow water carbonates of the Lower Jurassic Calcare Massiccio Fm. and syn-rift dolomitized pelagic micrite and calcarenites of the Lower Jurassic Corniola Fm. These Mesozoic rocks tectonically overlie the Circeo Flysch deposits along the NNE-verging Circeo thrust (Accordi, 1966; Pantosti et al., 1986). The flysch consists of glauconitic sandstones, calcarenites, and marls, and an Aquitanian age has been proposed for it, based on the occurrence of resedimented *Miogypsina* (Accordi, 1966). Despite its limited exposure, the Circeo thrust represents one of the major compressive structures of the Apennines, with a stratigraphic separation of about 2.5 km that is comparable with that of the major thrusts of the central and northern Apennines.

3. Methods and Data

3.1. Interpretation of Seismic Lines and Deep Wells

Two public seismic lines (Figures 2c and 3; www.videpi.com) were interpreted, limited to two key horizons and to only clearly evident faults, to avoid any over-interpretation of structures considering the low quality of the seismic lines. The top Messinian - base Pliocene boundary consists of evaporites and gypsum-arenites and forms a marked reflectors in seismic lines (e.g., Conti et al., 2017; Tavani, Cardello, et al., 2021). The boundary between

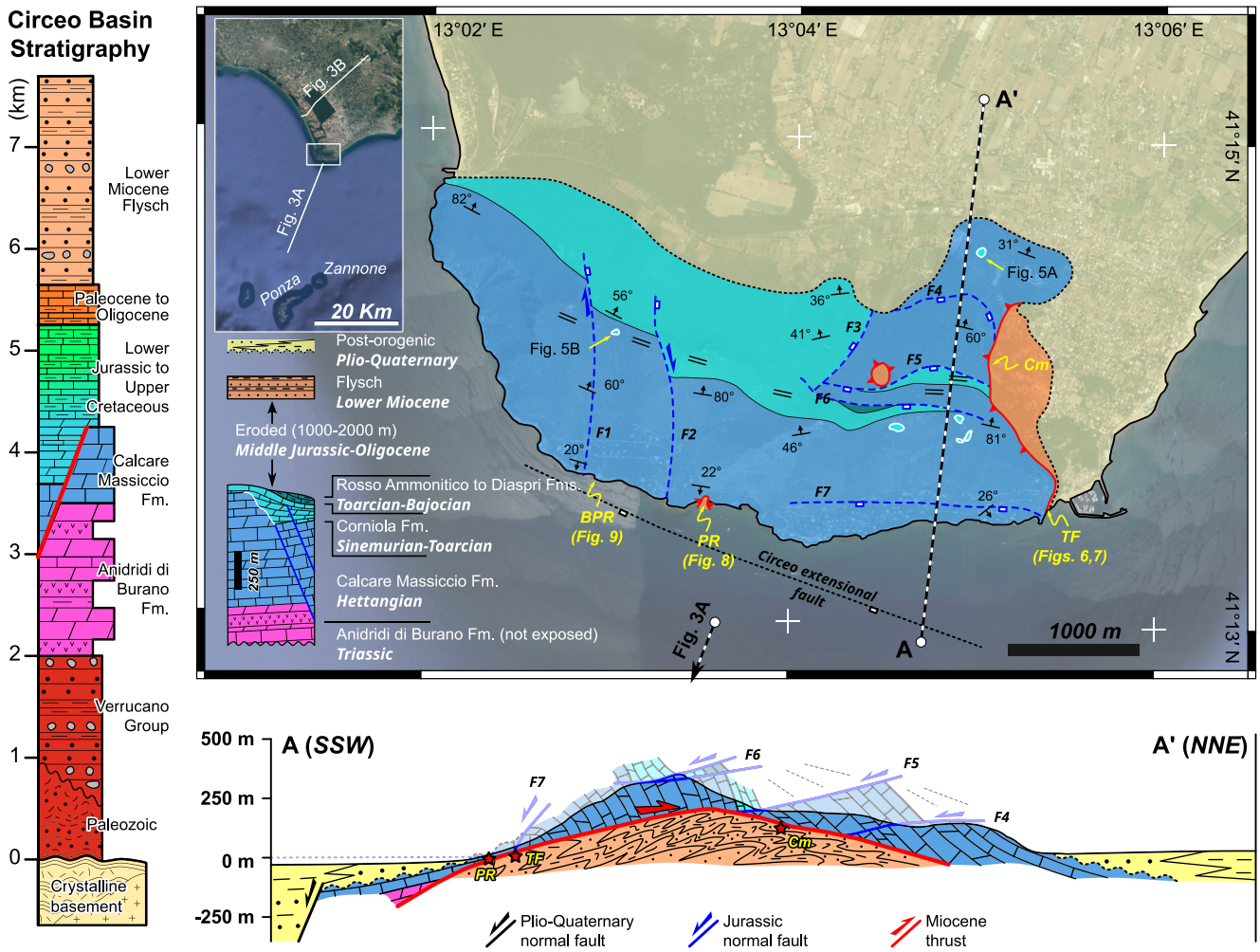

Figure 4. Geological map of the Circeo promontory, with N-S geological cross-section and stratigraphic succession of the Circeo pelagic basin; due to scale, only faults with offset exceeding 100 m are represented. BPR, Batterie di Punta Rossa site; PR, Punta Rossa site; TF, Torre fico site; Cm, Cemetery site.

the Meso-Cenozoic carbonates and the overlying syn-orogenic siliciclastic deposits is also a well-recognizable reflector, which in the case of the LT-329-86V onshore seismic line (Figure 3b) is further constrained by outcrops to the NE and by the Fogliano-1 well. It is worth noting that carbonates of the Circeo pelagic basin and of the adjacent slope domain are found in the Fogliano-1, Tre Cancelli-1, Michela-1 and Mara-1 wells, whereas carbonates exposed in the Volsci Range, crossed by the NE border of the onshore LT-329-86V seismic line, pertain to the Latium-Abruzzi carbonate platform (Figure 2). Therefore, the transition between these two paleogeographic domains, although not detectable, occurs along the LT-329-86V seismic line, NE of the projected Fogliano-1 well.

3.2. Geological Mapping

The geological map (Figure 4) builds on previous maps by Accordi (1966) and Cardello (2006). In the field, we have collected faults and bedding orientation and we have identified the stratigraphic boundary between four units: (a) the Lower Jurassic pre-rift Calcare Massiccio Fm.; (b) the Lower Jurassic syn-rift Corniola Fm.; (c) a thin unit that includes marls and cherts, coeval to the Lower-Middle Jurassic Rosso Ammonitico to Diaspri fms. interval of the Umbria-Marche succession; (d) the Circeo Flysch. The data were collected using the FieldClino App for Android.

3.3. Structural and Microstructural Analyses

Three outcrops have been studied in detail: the Torre Fico (TF) and the Punta Rossa (PR) outcrops of the Circeo Flysch in the footwall of the Circeo thrust and the damage zone of the offshore Circeo extensional fault at the

Batterie di Punta Rossa site (BPR) (Figure 4). We collected mesostructural data, including attitude of faults, joints, S, C, and C′ planes, and slickenlines, and defined crosscutting relationships between different structural elements. Microstructural analyses on polished thin sections with an optical microscope were used to determine the mechanisms of vein and slickenfiber precipitation and crosscutting relationships at the microscale.

3.4. Carbonate C, O, and Clumped Isotopes Geochemistry

At the TF site (Figure 4), 44 calcite slickenfibers of faults and S-like, C, and C′ planes were sampled from the deformed Circeo Flysch unit <5 m below the Circeo thrust. Seven additional samples were also collected in a small (~2 m wide) relatively undeformed exposure of the Circeo Flysch, 15 m to the north of the TF site of Figure 4. Samples powders were produced with a microdrill avoiding contamination of the calcite slickenfibers with the host rocks. The carbonate C, O, and clumped isotope values of the powdered calcites were determined at the Stable Isotope Laboratory of ETH Zürich using Thermo Fisher Delta V with GasBench II and Thermo Fisher Scientific MAT253 mass spectrometer coupled to a Kiel IV carbonate preparation device, following the method described in Schmid and Bernasconi (2010), Meckler et al. (2014), and Müller et al. (2017). During each run of the autosampler with 46 positions, 2 or 3 replicates (130–145 μg each) of different samples, 5 replicates of the carbonate standards ETH-1, ETH-2, and 10 replicates of the standard ETH-3 were analyzed with the LIDI method (Müller et al., 2017). All calculations and corrections were done with the software Easotope (John & Bowen, 2016) using the revised IUPAC parameters for ^{17}O correction as suggested by Daëron et al. (2016). The results are reported in the Intercarb carbon dioxide equilibrium scale (Bernasconi et al., 2021) with uncertainties reported at the 95% confidence level (Fernandez et al., 2017). Precipitation temperature (TΔ47) was calculated according to Anderson et al. (2021) and $\delta^{18}O$ of paleo-fluids according to O'Neil et al. (1969).

A limitation of carbonate clumped isotope thermometry is the possible modification of the original temperature due to solid-state bond reordering. In this case, the measured TΔ47 reflects an apparent temperature ranging between the original crystallization temperature and the maximum temperature experienced during burial (Henkes et al., 2014; Stolper & Eiler, 2015). Given the recent age of the calcite and the low temperature during maximum burial conditions after their formation, as illustrated in the results section, the models of Henkes et al. (2014) and Stolper and Eiler (2015) predict that such a reordering is negligible in our analyses.

Results of carbonate C, O, and clumped isotope analyses are stored in the Earthchem public repository (https://doi.org/10.26022/IEDA/112696). Carbon and oxygen isotope compositions are reported in the conventional δ notation respect to the Vienna Pee Dee Belemnite (V-PDB) for $\delta^{13}C$ and Vienna Standard Mean Ocean Water (V-SMOW) for $\delta^{18}O$, and in the running text ‰ will be used instead of ‰ V-PDB and ‰ V-SMOW. Notably, the V-SMOW value for the $\delta^{18}O$ is derived from the original V-PDB value (Sharp, 2007).

3.5. Calcite U-Pb Dating

We performed U-Pb radiometric dating on eight polished thin-sections representative of calcite slickenfibers coating five reverse C planes and three extensional fault planes from the TF site (Figure 4). Five samples (three reverse C planes and two extensional faults) have returned ages with errors below 10 Myr. U-Pb dating has been performed after cathodoluminescence microscopy observations (on the same sections) that showed that all the calcites are characterized by homogeneous red luminescence. This suggests single calcite precipitation events for all dated samples. The samples have been analyzed by LA-ICPMS at the Preston Cloud Laboratory, University of California, Santa Barbara (e.g., Nuriel et al., 2017). All the U-Pb data are stored in the Earthchem public repository (https://doi.org/10.26022/IEDA/112697 and https://doi.org/10.26022/IEDA/112904).

3.6. Nannoplankton Analysis

We collected eight samples from the Circeo Flysch (Localities PR, TF, and Cm in Figure 4) for nannofossil biostratigraphy, using smear slides (Bown & Young, 1998) and observed them at 1,000X magnification with a Zeiss Axioscop microscope.

3.7. Stratimetry of the Circeo Pelagic Basin, Cross-Section Balancing, and Forward Modeling

The 48 km long balanced cross-section is built along a N29° striking vertical plane (trace in Figure 2c), using the 3DMove software (Petex). The N29° strike is chosen to average the tectonic transport direction of major

Table 1
Summary of Mineralogical X-Ray Diffraction Analyses for the Circeo Flysch Sampled at the Punta Rossa, Torre Fico, and Cemetery Sites

					X-ray semiquantitative analysis of the <2 μm grain-size fraction (%wt.)						
Sample	Latitude	Longitude	Formation	Rock type	I	I-S	Kln	Chl	Non clay minerals	*R*	%I in I-S
Punta Rossa (PR)	41.22504	13.059003	Flysch	Sandsone	21	38	37	4	Qtz	1	70
Torre Fico (TF)	41.22497	13.090233	Flysch	Sandsone	55	15	–	30	Qz, Cal, Ab	1	75
Punta Rossa (PR)	41.22504	13.059003	Flysch	Sandsone	39	44	–	17	Qz, Cal, Ab	0/1	30/70
Cemetery (Cm)	41.23422	13.084386	Flysch	Sandsone	51	49	–	–	Qz, Cal, Ab	3	80

Note. Sm = I = illite; I-S = mixed layer illite-smectite; Kln = kaolinite; Chl = chlorite; Qz = quartz; Cal = calcite; Ab = albite; *R* = stacking order (Jagodzinski, 1949); %I in I-S = illite content in mixed layer illite-smectite.

structures in the Apennines and the local strike of structures in the Circeo promontory (N100-110°). In its central portion, the balanced cross-section completes at depth the surface section of Figure 4, whereas to the north and to the south it is built taking into consideration the major features observed in the seismic lines of Figure 3. The seismic lines and the geological cross-section are projected perpendicular to the trace of the balanced cross-section whereas, due to its distance, the Fogliano-1 well is projected along the direction N135°, the main strike of the typical Apenninic structures. Line-length preservation (<1.5% of restored length error), and flexural-slip folding are assumed during restoration (e.g., Dahlstrom, 1969; Hossack, 1979). The reconstruction is further validated by means of forward modeling, focused only on the thrusting stage. Modeling applied the fault-bend folding algorithm of 3DMove (i.e., the implementation of the flexural-slip fault-bend folding model; Suppe, 1983) to faults that are derived from a simplified version of the restored balanced cross-section.

To construct the balanced cross-section, we built a simplified stratigraphic section for the Circeo pelagic basin (Figure 4), including literature data and constraints from seismic lines of Figure 3, wells in Figure 2b, and cross-section of Figures 1–4. The ~7 km thick Triassic to Miocene sedimentary package and the underlying Paleozoic phyllites and quartzites (Vai, 2001) have been subdivided into six groups which are on top of the rheologically stiff Variscan crystalline basement of Adria (Figure 4): The lowermost group is made by Paleozoic phyllites and quartzites and by the Triassic continental red beds of the Verrucano group, and its thickness is 2 km. The overlying group includes the 1.5 km thick Triassic Anidriti di Burano Fm. On top of this, the Lower Jurassic pre-rift Calcare Massiccio Fm. is 750 m thick. The fourth group is 1.5–1.8 km thick, and it is made by Early Jurassic syn-rift and Middle Jurassic to Upper Cretaceous post-rift pelagic carbonates. These sediments are capped by 400–500 m of Cenozoic pre-orogenic deep-water marls and limestones. On top of this pre-orogenic succession, the seventh group is made by the 2.2 km thick Circeo Flysch. Details on the data used to build the stratigraphic succession of the Circeo basin are provided in Supporting Information S1.

Timing of major thrusts and subsequent extensional faulting is provided by thermochronological data from the TF (Fellin et al., 2022), and it is further constrained by our burial modeling and U-Pb dating.

3.8. X-Ray Diffraction of Clay Minerals as Constraint for Burial and Thermal Modeling

We collected four sets of samples from the Lower Miocene Circeo Flysch (Localities PR, TF, and Cm in Figure 4) for XRD of clay minerals to constrain the burial and thermal modeling (Table 1). XRD analysis of the <2 μm fraction was carried out with a Scintag X1 X-ray system (CuKα radiation) at 40 kV and 30 mA. The <2 μm fraction was separated from the bulk rock by centrifuging, and sedimented on glass slides producing a thin aggregate of at least 3 mg of clay per cm^2. These samples were air-dried at room temperature overnight and then saturated in ethylene-glycol atmosphere at 25°C per 24 hr. Oriented air-dried and ethylene-glycol solvated samples were scanned from 1 to 48°2θ and from 1 to 30°2θ, respectively, with a step size of 0.05°2θ and a count time of 4 s per step. The illite content in mixed layers illite-smectite (I-S) was determined according to Moore and Reynolds (1997), using the delta two-theta method after decomposing the composite peaks between 9 and 10°2θ and 16–17°2θ. The I–S ordering type (Reichweite parameter, R; Jagodzinski, 1949) was determined by the position of the I001-S001 reflection between 5 and 8.5°2θ (Moore & Reynolds, 1997). Peaks in relative close position were selected for clay mineral quantitative analysis in order to minimize the angle-dependent intensity effect. Composite peaks were decomposed using Pearson VII functions and the WINXRD Scintag program.

Integrated peak areas were transformed into mineral concentration by using mineral intensity factors as a calibration constant (Moore & Reynolds, 1997).

Two reconstructions of the burial and thermal history of the Circeo Flysch at the footwall of the Circeo thrust were carried out using the software package Basin Mod® 1-D (1996). The main assumptions were: (a) rock decompaction factors apply only to clastic deposits (Sclater & Christie, 1980); (b) seawater depth variations in time are assumed not to be relevant, because thermal evolution is mainly affected by sediment thickness rather than by water depth (Butler, 1992); (c) thrusting age was constrained by U-Pb dating of syn-kinematic contractional calcite slickenfibers; (d) thermal modeling is performed using LLNL Easy %Ro method based on Burnham and Sweeney (1989) and Sweeney and Burnham (1990); (e) exhumation is considered linear for given time intervals and is constrained by thermochrolonogical data (Fellin et al., 2022); (f) geothermal gradient is assumed to be 25°C/km during compressional deformation and subsequent extension, consistently with Fellin et al. (2022). Thicknesses of units are based on lithostratigraphic columns of geological maps and field observations (Section 3.7). Mixed layers I-S were converted into vitrinite reflectance-equivalent values by the maturity conversion tool of Basin Mod® 1-D, and by the correlation of vitrinite reflectance and expandability (reverse of illite content in I-S) data. The latter is based on the kinetic model of vitrinite maturation of Burnham and Sweeney (1989) and the kinetics of the I-S reaction determined by Hillier et al. (1995).

4. Results

4.1. Seismic Interpretation

Offshore, in seismic line E-174 (Figure 3a), the top carbonate reflector defines a gentle apparent SW-dipping monocline affected by three major normal faults. The south-western fault is the largest one and, in its footwall, the 0.5 s-thick syn-orogenic package overlying the top carbonate reflector connects with the syn-orogenic unit exposed in the footwall of the Zannone thrust. The sub-horizontal top Messinian/base Pliocene reflector is extensionally faulted. The package between the top carbonates and the top Messinian pinches out in NE direction. The overlying Plio-Quaternary sediments seal the extensional faults, dating faulting at the Pliocene interval. On the other hand, wedging of the package comprised between the top carbonate reflector and the top Messinian/base Pliocene reflector indicates that tilting of the top carbonate reflector is pre-Messinian.

Onshore, in seismic line LT-329-86V (Figure 3b), the top carbonate reflector forms an apparent SW-dipping monocline and, in the SW portion of the line, it defines a structural step of about 1 s, as constrained by the Fogliano-1 well. This is interpreted as a fault-related fold due to a SW-dipping thrust. In fact, between kilometers 8 and 14 along the section, the occurrence of an extremely thin-sequence of Plio-Quaternary sediments filling a gentle basin rules out a Pliocene NE-dipping fault with a displacement of 1 s. This framework suggests the chaotic shallow reflectors between kilometers 2 and 8 to be associated with folding and thrusting ahead of a major thrust, tentatively indicated in our interpretation (Figure 3b).

4.2. Geological Map and Cross Section

Mesozoic carbonates in the hanging wall of the Circeo thrust are subvertical to steeply NNE-dipping in the central portion of the Circeo promontory. They become moderately NNE-dipping toward the north and gently S-dipping in a narrow ribbon along the southern portion of the promontory (Figure 4), thus defining an E-W trending anticline-syncline pair. Unconformable contacts between Jurassic pre-rift Calcare Massiccio and syn-rift Corniola fms. (Figure 5) document Early Jurassic fault paleoescarpments, indicative of extensional growth faults with displacements of hundreds of meters. These faults, tilted and folded during shortening, are labeled F1 to F7 in Figure 4. It is worth noting that in the unconformable contacts between the Corniola and the Calcare Massiccio fms. (Figure 5), when the bedding of the Corniola Fm. is restored to the horizontal, the bedding of the Calcare Massiccio Fm. becomes N-dipping. This relationship suggests block-tilting during Jurassic faulting. Overall, the inferred Jurassic faults, in their original orientation, form N-S and E-W striking sets, which are the well-constrained orientations of syn-rift Jurassic fault exposed in the central Apennines (see Section 2.2).

4.3. Structural and Microstructural Analyses

The TF site (Figure 4) is the largest and best-preserved exposure of the Circeo thrust (Figure 6). There, the Circeo Flysch in the footwall damage zone is affected by a well-developed C-C′ fabric (Figure 7) providing a top-to-NNE

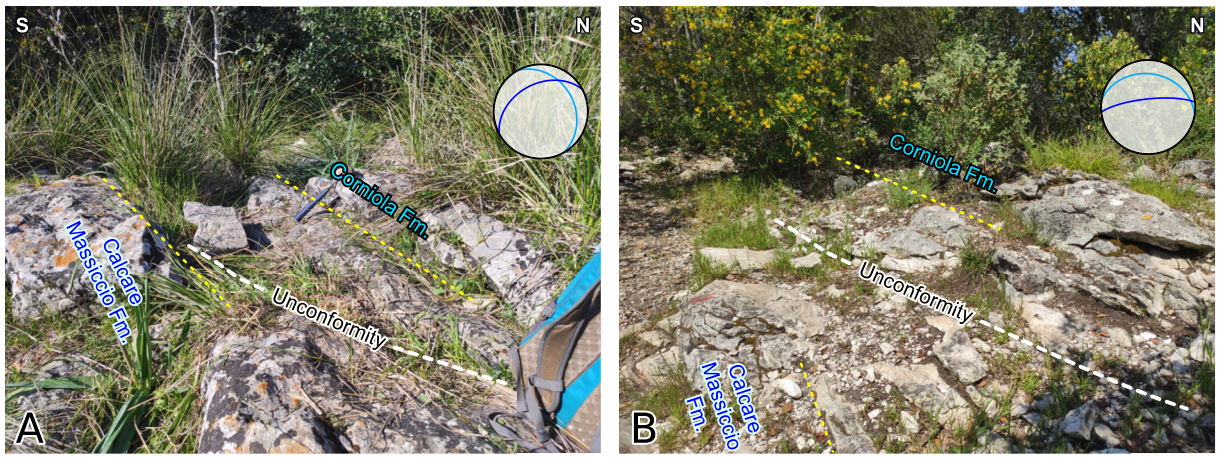

Figure 5. Field photos of unconformable contacts between the syn-rift Corniola Fm. and the pre-rift Calcare Massiccio Fm. (location of the photographs is indicated in Figure 4).

shear sense (Figures 7a and 7b). S-like structures, defined by reverse structures oriented at 45° with respect to the C planes and providing the same shear sense as the C, also occur (Figure 7c). This fabric is cut by high-angle (Figure 7c) and low-angle (Figure 7d) normal faults, with calcite slickenfibers indicating a SSW-directed general shear sense (Figure 6). As observed in the stereoplot (Figure 6) and in Figure 7d, the gently-dipping C planes of the NNE- and SSW-verging sets are essentially parallel to each other. The Calcare Massiccio Fm. in the hanging wall of the thrust is affected only by extensional faults, which have striations indicating NNE-SSW extension (Figure 6). At the TF site, the thrust is not displaced by extensional faults. In addition, the thrust plane is parallel to SSW-directed low-angle normal faults observed in its footwall. This indicates that the pervasive fabrics of extensional structures affecting the footwall and hanging wall emanate from the thrust zone. This provides robust evidence of its negative inversion. Calcite slickenfibers coating S-like, C, and C′ planes and the normal faults are characterized by multiple crack and seal shear veins bounded by sharp slip planes, giving the shear veins a striped

Figure 6. Panoramic view of the Circeo thrust at the Torre Fico site, with the steeply N-dipping layers of the Lower Jurassic Calcare Massiccio Fm. in the hanging wall, and the Lower Miocene Circeo Flysch in the footwall. Steroplots of mesostructures collected in the footwall and hanging wall are displayed.

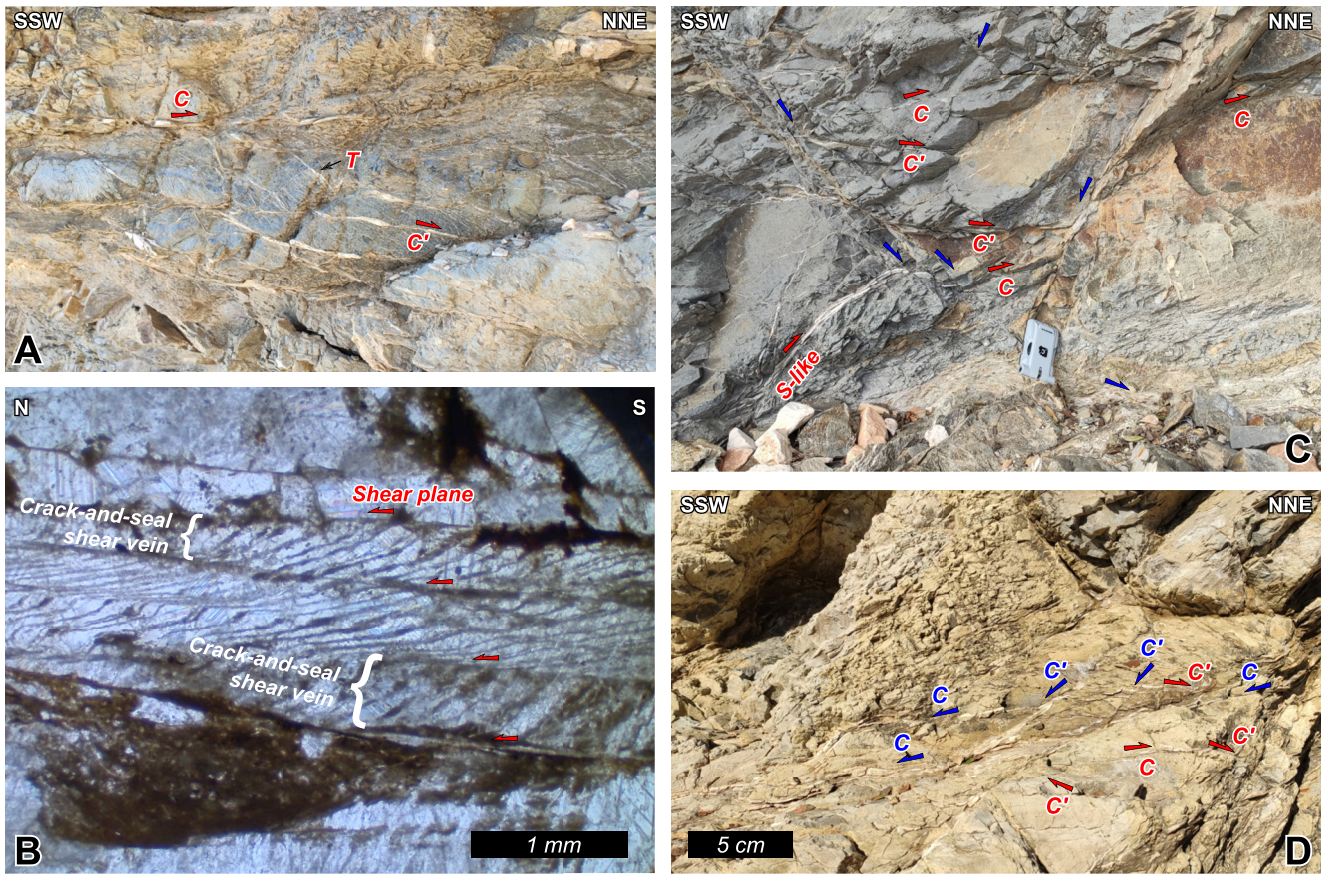

Figure 7. Footwall damage zone of the Circeo thrust at the Torre Fico site (location is indicated in Figure 4). (a) C/C′ and T structures associated with a top-to-NNE shear. (b) Microphotograph of a S-like structure showing crack-and-seal shear veins bounded by shear planes. (c) NNE-verging S-like-C/C′ structures offset by conjugate normal faults. (d) NNE-verging C/C′ fabric postdated by SSW-verging C/C′ fabric.

appearance (e.g., Cerchiari et al., 2020; Dielforder et al., 2016; Koehn & Passchier, 2000) (Figure 7b). Calcite fills micrometer-thick dilational jogs, suggesting incremental void opening during multiple slip events.

At the PR site (Figure 4), the thrust plane is exposed in a 1 m wide exposure (Figure 8a). About 30 m to the east of this area, a 10 m wide exposure of the Circeo Flysch, oriented perpendicular to the thrust shear sense, is characterized by S-like-C/C′ structures and some extensional structures (Figures 8b and 8c). The strata in the footwall of the thrust are affected by S-like-C/C′ fabric with a top-to-NNE vergence (Figure 8b). There, the Circeo thrust is displaced by a SE-dipping normal fault (Figure 8b), which juxtaposes the Calcare Massiccio Fm. (originally in the hanging wall of the Circeo thrust) onto the Circeo Flysch (in the footwall of the thrust). The Circeo Flysch is also affected by NE-SW and NW-SE striking joints and normal faults (Figures 8b and 8c), that is, both parallel and perpendicular to the major normal fault displacing the thrust.

At the BPR site (Figure 4), the damage zone of the offshore Circeo extensional fault affects the Calcare Massiccio Fm. This damage zone consists of closely-spaced (i.e., ∼1–2 m) normal faults (Figure 9a), some having a cm-thick cataclastic fault core (Figure 9b). These faults are mostly NE dipping, that is, antithetic to the major fault, and indicate NE-SW oriented extension (Figure 9b). No other exposures of the Calcare Massiccio Fm. in the Circeo promontory are characterized by the occurrence of similar highly-strained fault rocks.

4.4. Carbonate Carbon, Oxygen, and Clumped Isotope Geochemistry

Due to the small size (i.e., ∼2 m wide) of the portion of TF exposure where the flysch is undeformed, the seven $\delta^{13}C$ and $\delta^{18}O$ values for the host rock are considered the host-rock counterpart for all the values of calcite slickenfibers. This allows us to consider Figure 10a as a cross plot of the isotopic value of host rock versus

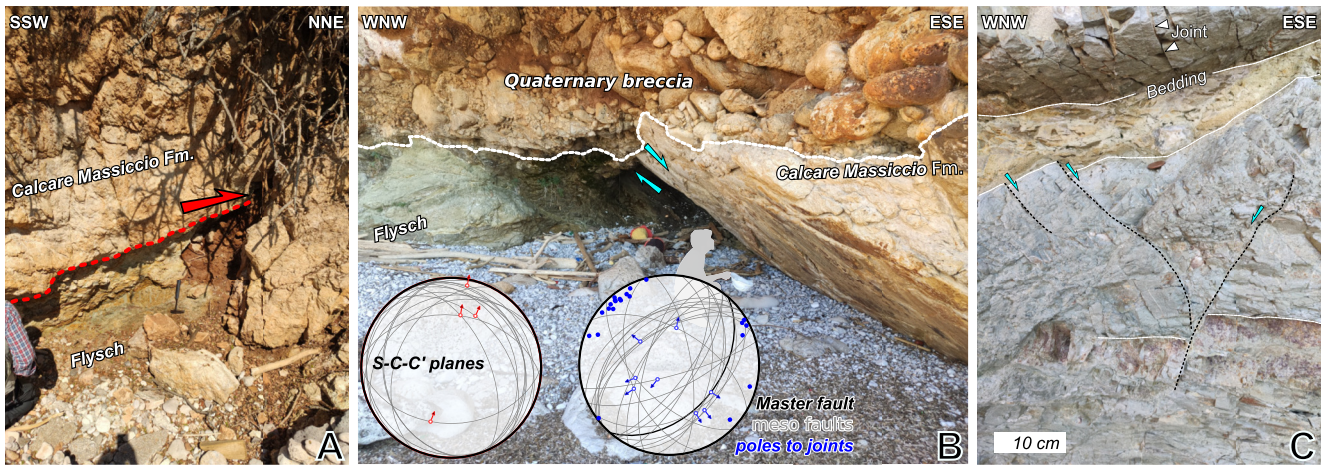

Figure 8. Circeo thrust at the Punta Rossa site (location is indicated in Figure 4). (a) Photo of the contact. (b) Footwall damage zone with the NE-SW striking normal fault displacing the thrust and putting in contact the Circeo Flysch in the footwall of the Circeo thrust with the Calcare Massiccio Fm. in its hanging wall. Steroplots of S-like-C/C′ fabric and joints and normal faults affecting the flysch are displayed, with the major fault plotted with a thick black line. (c) Detail of the joints and normal faults in the flysch.

slickenfibers, for both C and O. The host rock shows $\delta^{13}C$ values between −1.0 and +0.5‰, and $\delta^{18}O$ values between +27.0 and +28.0‰. The slickenfibers of NNE-verging S-like, C and C′ fabrics and of SSW-verging extensional faults form a well clustered group characterized by $\delta^{13}C$ values between −1.5 and +0.5‰, and $\delta^{18}O$ values between +24.0 and +26.5‰ (Figure 10a). NNE-verging slickenfibers on S-like, C, and C′ planes show TΔ47 of ∼100°C–110°C (Figure 10b). The SSW-verging slickenfibers on extensional faults show TΔ47 of 99°C, 126°C and 135°C (Figure 10b).

Overall, slickenfibers show $\delta^{13}C$ values comparable with those of the Circeo Flysch and average $\delta^{18}O$ values ∼2.0‰ lower than the average of the host rock. Calculated $\delta^{18}O$ of the mineralizing fluids are between 8.5 and 13‰ (Figure 10b), corresponding to fluids with high degree of interaction with the host rock (e.g., Beaudoin et al., 2020; Curzi, Aldega, et al., 2020). The NNE- and SSW-verging sets have identical $\delta^{13}C$ and $\delta^{18}O$ values, but slightly different TΔ47: the SSW-verging extensional mineralizations are ∼10–20°C warmer than the NNE-verging compressive mineralizations but within the uncertainty of the measurements (Figure 10b).

4.5. U-Pb Dating of Calcite Slickenfibers and Relative Timing Between Shearing Events

Slickenfibers coating NNE-directed C planes yield ages of 15.6 ± 1.9 Ma, 14.3 ± 1.3 Ma, and 12.7 ± 2.0 Ma (Figure 11). The SSW-directed normal faults showed an age of 15.8 ± 6.7 Ma for a slickenfiber coating an extensional fault plane (sample 57 in Figure 11) and 13.6 ± 7.2 for an array of veins in the dilatation jog of an

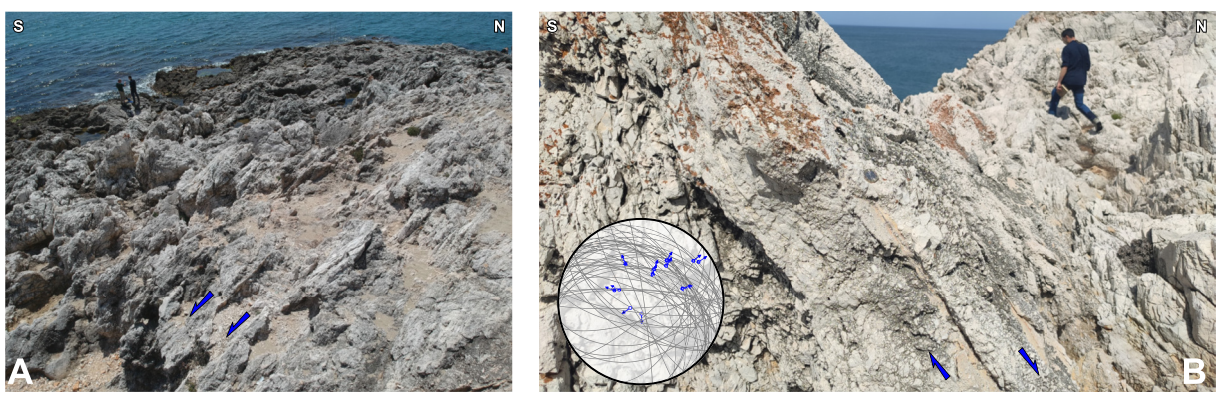

Figure 9. Damage zone of the Circeo extensional fault at the Batterie di Punta Rossa site (location is in Figure 4). (a) View of the array of normal faults affecting the Calcare Massiccio Fm. (b) Detail of a normal fault, with a cataclastic fault core, and stereoplot of faults collected at the site.

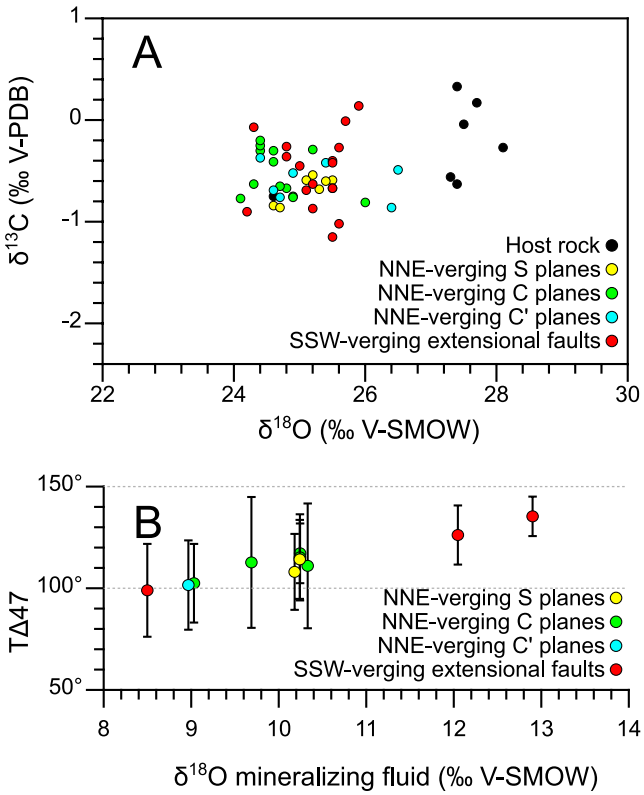

Figure 10. Geochemical results sorted on the basis on different types of samples. (a) Scatter plot of $\delta^{18}O$ (Vienna Standard Mean Ocean Water) versus $\delta^{13}C$ (Vienna Pee Dee Belemnite) diagram. (b) TΔ47 and uncertainty in 95% confidence levels obtained following Anderson et al. (2021) versus calculated $\delta^{18}O$ of paleo-fluids.

high angle normal fault (sample CC1 in Figure 11). Dates from three other samples with uncertainties >10 Ma are not discussed. All the slickenfibers/veins showed homogeneously dull cathodoluminescence (Figure 11), ruling out mineralization from different fluids.

As reported in Section 4.3, at the TF site, where samples for U-Pb dating have been collected, we observe that NNE-verging structures are constantly crosscut by SSW-verging extensional structures. However, no direct crosscutting relationships between the analyzed samples is observed at the microscale.

Given the above illustrated data and errors, two end member scenarios will be discussed for the intervals during which the compressional and extensional structures were active. These scenarios consider large and short time intervals for thrusting and large and short time intervals between the onset of compression and extension. In the first scenario, compression along the Circeo thrust lasted from 17.5 until 10.7 Ma, and negative inversion of the thrust started at 9.1 Ma. In the second scenario, thrusting started at 15.6 Ma and terminated at 12.7 Ma, when the thrust started to be negatively inverted.

4.6. Nannoplankton Analysis

In most samples the nannofossils in the flysch at the footwall of the Circeo thrust are scarce and moderately preserved, with reworked forms. Overall, the few recognized specimens do not allow the definition of a restricted biostratigraphic range. In the following we consider the age of this formation bracketed to the Aquitanian (occurrence of resedimented Miogypsina; Accordi, 1966) to Burdigalian (consistent with the oldest U-Pb age for the Circeo thrust) period.

4.7. Balanced Cross Section and Forward Kinematic Modeling

The balanced cross-section in Figure 12 was built assuming a gently NE-dipping regional dip, coherent with the local NE dip of the Moho (Di Stefano et al., 2011) generated by crustal thinning associated with the opening of the Tyrrhenian back-arc basin. The northern portion of the section is characterized by a wide SW-dipping monocline, minimally affected by extensional faults, as derived by the continuity of the top carbonate reflector observed in the seismic line of Figure 3b. This monocline forms the backlimb of the Volsci Range thrust sheet and involves the 2.5–3 km thick Lower Jurassic to Upper Cretaceous sedimentary succession of the Latium-Abruzzi carbonate platform, unconformably overlain by the Miocene syn-orogenic succession. Determining with accuracy the position of the branch point of the Volsci Range thrust is out of the scope of this work, and consequently bed lengths in the footwall of this thrust are not computed in the restoration of the section. In the central and SW portions of the section, four major extensional faults are observed in the offshore seismic line of Figure 3a. These faults have produced a downthrow of the southern portion of the section of about 2 km, as indicated by the occurrence of the Anidriti di Burano Fm. just one hundred meters below the surface (Figure 4), whereas in the Michela-1 well, the formation has been encountered at a depth of 2 km (Figure 2b). Consequently, the base of the Calcare Massiccio Fm. between the two areas is offset by 2 km, at least. Owing to the remarkable extensional displacement, we assume that the extensional system displaces the basal thrust and penetrates the basement. The northern extensional fault has SW-dipping carbonates in its hanging wall, as observed in the northern portion of the seismic line in Figure 3b. These SW-dipping layers form the backlimb of the Circeo anticline, whose crest and forelimb are exposed at the Circeo promontory (Figure 4). The doming of the Circeo thrust is caused by the development of the underlying anticline, associated with a frontal thrust connected with the thrust found at the bottom of the Mara-1 well (Figure 2b), that is, the Mara thrust. The development of the Mara thrust has caused the steepening of the ramp of the Circeo thrust. In our reconstruction, such a steepened ramp was negatively inverted and constitutes the central portion of the northern extensional fault (i.e., the Circeo Extensional fault in Figure 4). Jurassic extensional faults exposed in the field have been mostly crosscut by the Miocene thrust system although,

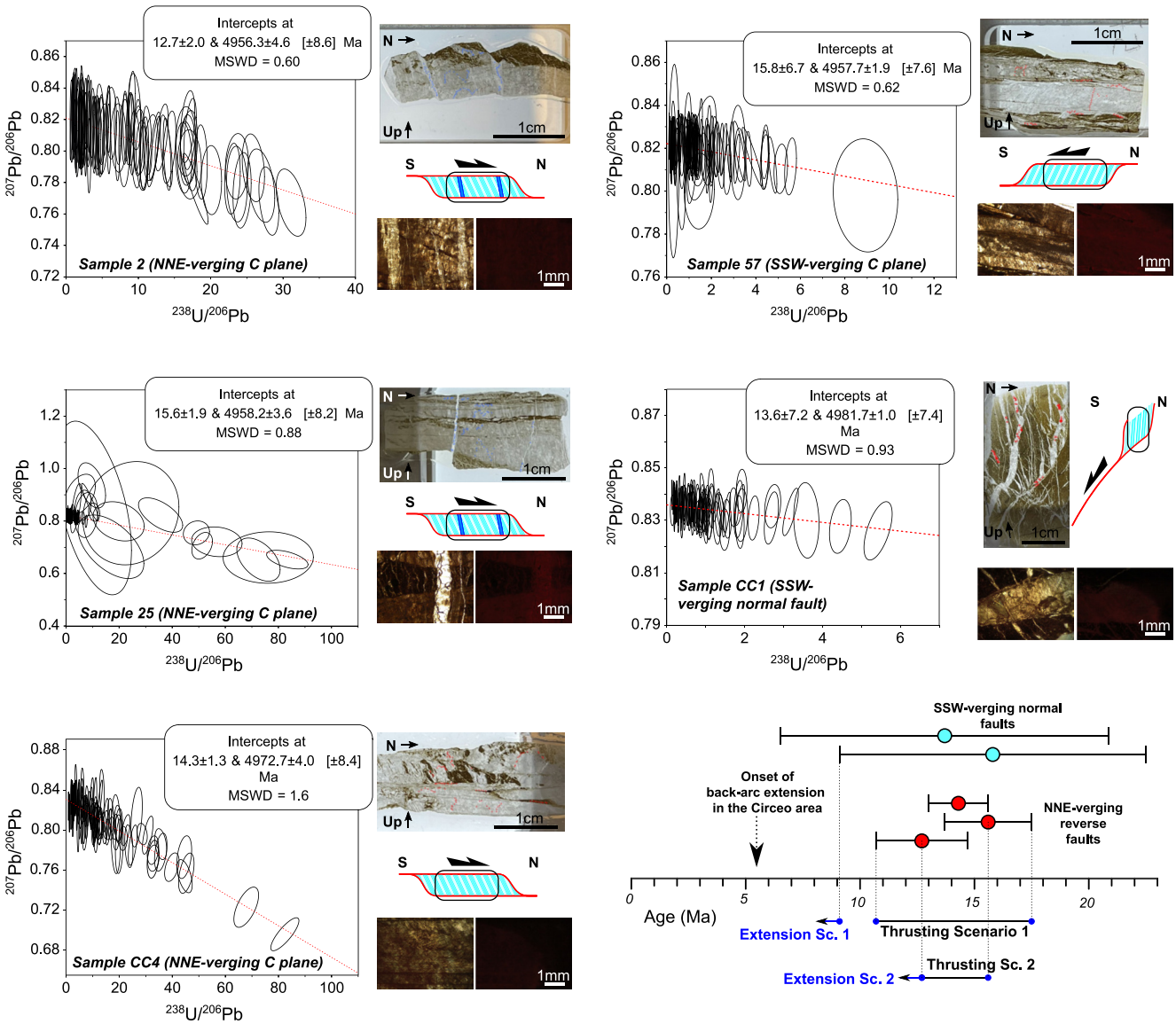

Figure 11. Plates of the five dated samples and relative diagram illustrating the age of compressive and extensional structures. Each plate includes: thin section of samples used for U-Pb dating with spots location; U–Pb Tera-Wasserburg plots; scheme showing the microstructure of the analyzed sample; details in both optical microscope and cathodoluminescence of syntectonic carbonates. Red line in the Tera-Wasserburg plots is the regression line that intercepts the concordia curve. MSWD: mean square weighted deviation.

based on the balanced cross section, we speculate that some segments of this Jurassic extensional system have been reactivated and positively inverted upon thrusting. The amount of shortening in the whole section is 9.8 km, whereas post thrusting extension is 2.3 km.

The balanced cross section is further validated by forward kinematic modeling (Figure 13) of a simplified version of the restored section of Figure 12. The thrust system developed in a piggy back sequence, with the inner Circeo thrust and the outer Mara thrust having displacements of 7,000 m and 2,600 m, respectively. Notably, the central part of the Circeo thrust, whose original dip was ~28°, steepened up to ~51° after the activation of the Mara thrust. Forward modeling highlights also the occurrence of a slight length deficiency in the upper thrust sheet during the development of the lower thrust, which is a well-known issue in fault-bend folds (e.g., Figures 21 and 22 in Suppe (1983)). The length deficiency is marked by the inclined loose line in Figure 13. Such a length deficiency in the forward modeling (which is coherent with the extra length in the same stratigraphic interval in the balanced cross section of Figure 12), requires syn-thrusting line lengthening and, ultimately, stretching in the

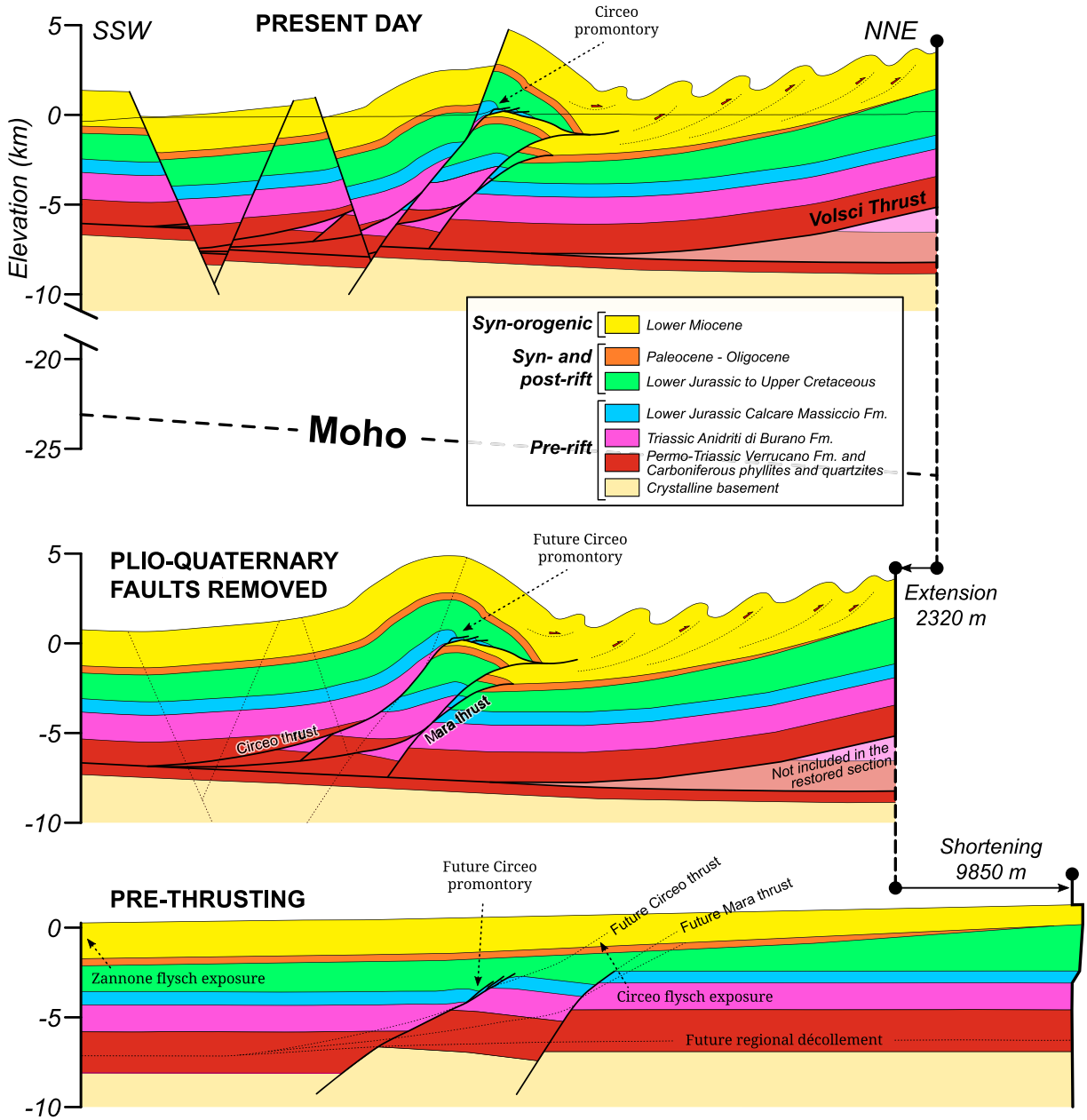

Figure 12. Balanced cross section (section trace is illustrated in Figure 3), with Pliocene faults removed and pre-thrusting restoration.

upper part of the Circeo thrust hanging wall during activation of the Mara thrust. This, coupled with the observed high dip of the Circeo ramp (~51°), is compatible with the extensional reactivation of the Circeo thrust already during the development of the Mara thrust, as illustrated in the inset of Figure 13.

4.8. Burial and Exhumation History

We evaluated two end-member scenarios for the burial evolution of the Circeo Flysch in the footwall of the Circeo thrust. As previously mentioned, scenario 1 considers a large time interval between tectonic burial and onset of exhumation that occurs 1.6 Ma after the end of burial, and includes the following steps (Figure 14): (a) deposition of 2.2 km (~2.5 km after decompaction) thick flysch unit between 23 and 17.5 Ma (see Section 4.6); (b) emplacement of the 4.1 km-thick Circeo thrust sheet between 17.5 and 10.7 Ma (as constrained by U-Pb ages for contractional slickenfibers) and contextual unroofing of about 2 km of flysch (i.e., creation of a 2.1 km elevated

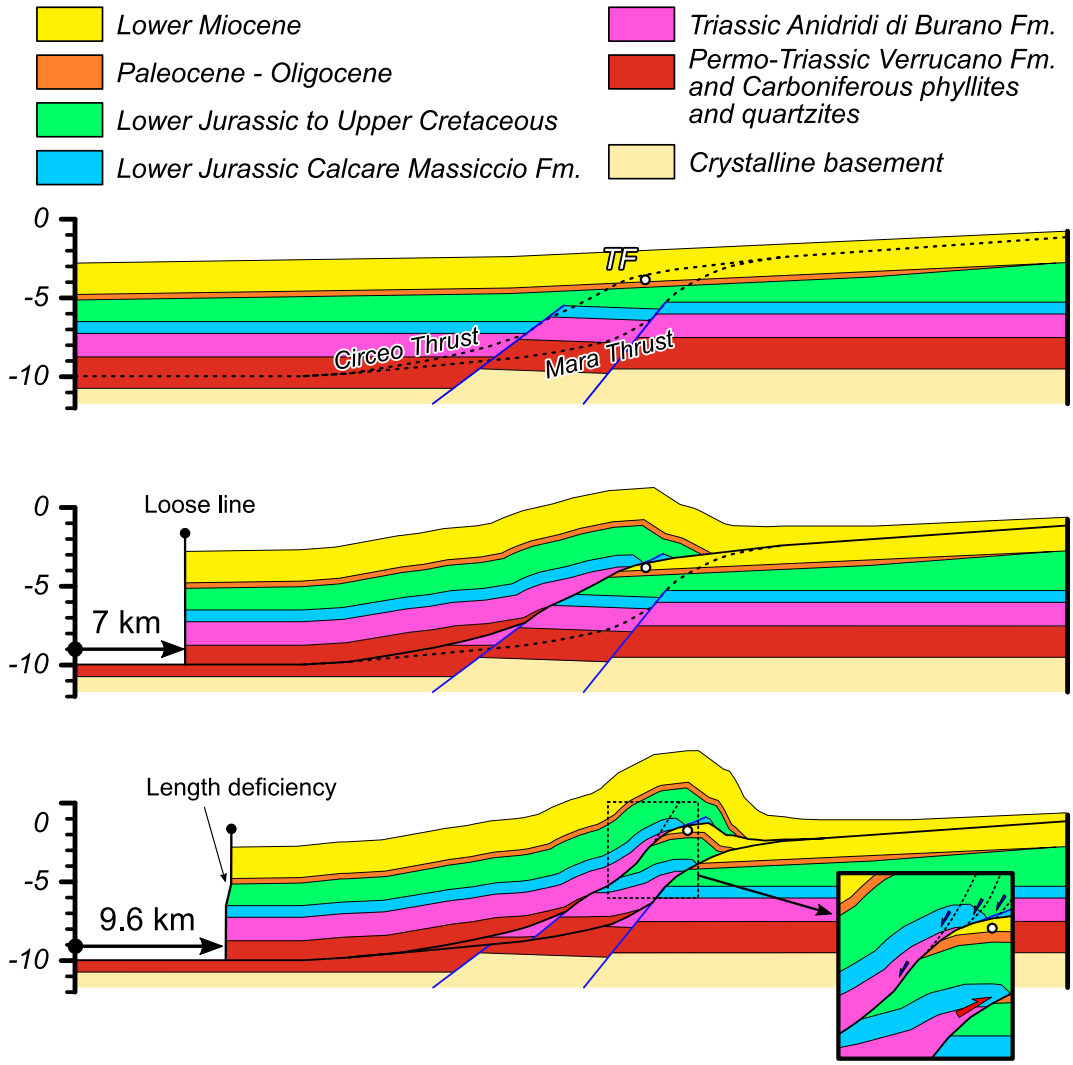

Figure 13. Forward kinematic modeling, with the inset showing the inception of gravitationally-induced extension at the end of the stacking.

ridge); (c) maximum burial conditions between 10.7 and 9.1 Ma; (d) uplift and erosion of about 2,000 m hanging wall unit between 9.1 Ma and 5.8 Ma. In scenario 2, tectonic burial occurs in a short time interval and exhumation starts immediately after it. The key steps in this scenario are: (a) deposition of 2.2 km (~2.5 km after decompaction) thick flysch unit between 23 and 15.6 Ma; (b) emplacement of the 4.4 km-thick Circeo thrust sheet between 15.6 Ma and 12.7 Ma (with the contextual tectonic removal of about 2,000 m of flysch) with maximum burial depth at 12.7 Ma; (c) instantaneous shift from compression to extension at 12.7 Ma, with uplift and erosion of about 2,000 m hanging wall unit between 12.7 and 5.8 Ma. In both scenarios, the final step is the exhumation of the flysch since 5.8 Ma, as constrained by A-He data by Fellin et al. (2022), indicating a cooling temperature of about 60° at that time.

Both scenarios fit mixed layer I-S data (thus no preference can be established based on thermal modeling), predict maximum burial temperatures of nearly 120°C, and are consistent with our stratimetric reconstruction.

5. Discussion

5.1. The Circeo Thrust System

According to our reconstruction, the Circeo promontory is an antiformal stack, *sensu* McClay (1992), similar to those developed in the outer central Apennines (e.g., Storti et al., 2018). The stack is made by the Mara thrust,

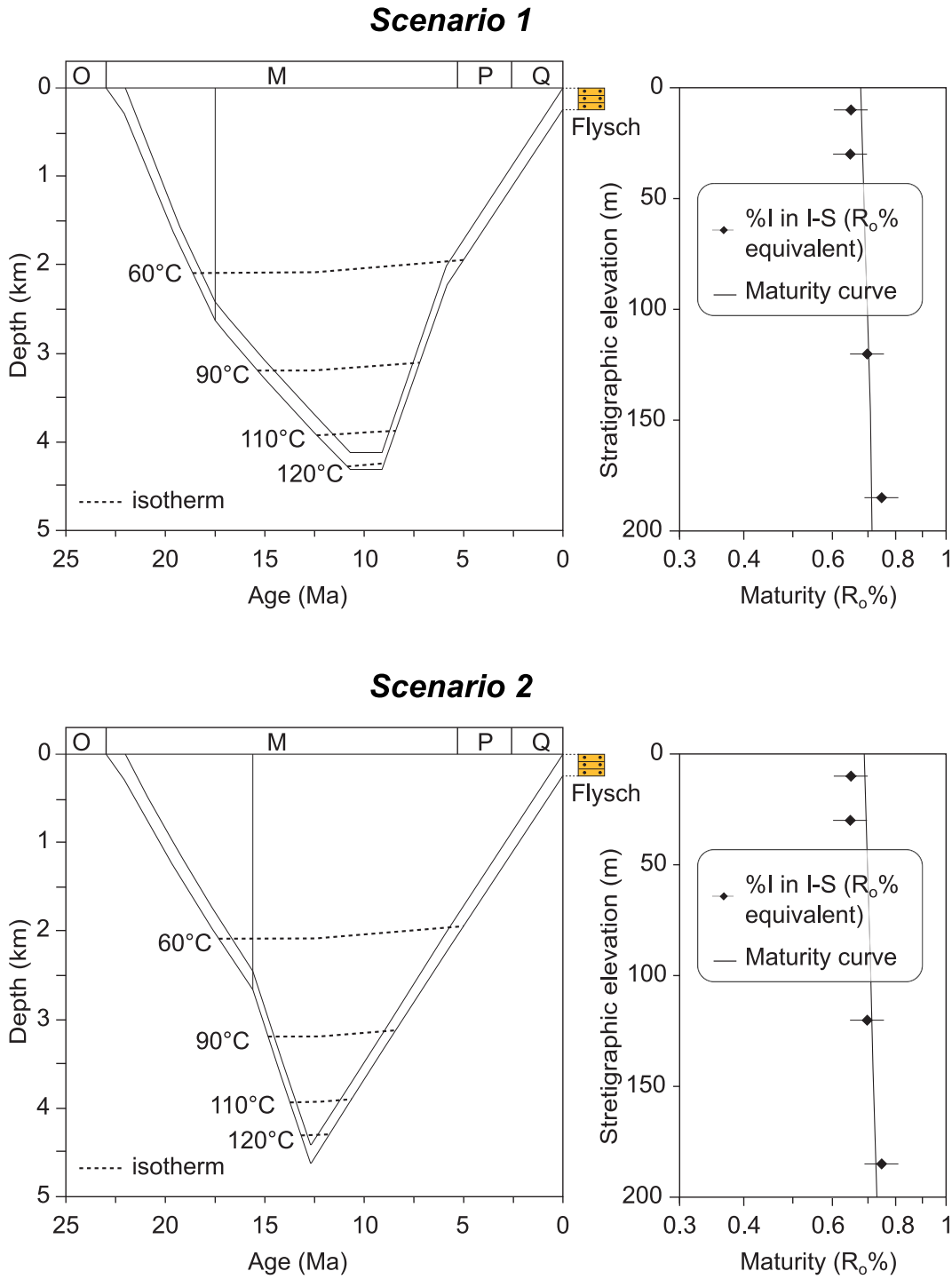

Figure 14. One-dimensional burial and thermal model for the exposed sedimentary succession of the Circeo Flysch at the footwall of the Circeo thrust (left graph) and thermal maturity curve calibrated against illite content in mixed layer I-S converted into vitrinite reflectance-equivalent values (R_o%) (right graph) for the two scenarios discussed in the text.

which folded and domed the overlying Circeo thrust (Figures 12 and 13). These thrusts together accommodated almost 10 km of shortening and both branch from a basal décollement located within the Verrucano group and the underlying metasedimentary rheologically weak units (Figure 4). A deeper sole thrust, and thus a significant involvement of basement rocks, is excluded given the short wavelength of folding of the Circeo thrust. The thrust system cuts and partly reuses syn-rift Early Jurassic faults exposed as paleoescarpments at the Circeo promontory

(Figure 5). These rotational Early Jurassic faults with ~1 km displacement formed part of the boundary of the Circeo pelagic basin. Pliocene extension with ~2 km of crustal stretching postdated thrusting and was accommodated by faults that in our view cut and displaced the basal décollement of the thrust system.

5.2. Syn-kinematic Fluid Circulation

The thrust-related and extension-related slickenfibers along the Circeo thrust have similar carbon and oxygen isotope values (Figure 10). The similar $\delta^{13}C$ values of slikenfibers and host rock and the calculated $\delta^{18}O$ value of paleo-fluids (ranging between 8.5 and 13‰), suggest intense fluid-rock interaction during the two shearing events (NNE- and SSW-verging). This indicates a closed fluid-circulation system, as already documented in the Apennines (e.g., Beaudoin et al., 2020; Curzi, Aldega, et al., 2020) and in other fold-and-thrust belts worldwide (e.g., Beaudoin et al., 2015). Moreover, since the TΔ47 values for both events are consistent with the assessed maximum burial temperature, we tend to exclude a significant contribution of deeply sourced exogenous fluids. The similar $\delta^{13}C$, $\delta^{18}O$, and TΔ47 values of extensional and compressional slickenfibers, support the idea that the SSE-directed extensional structures occurred at the same environmental condition as the NNE-directed compressional, likely with a very short delay between the two events.

5.3. Timing of Thrusting and Extension

The Circeo thrust zone is characterized by NNE-verging meso-structures postdated by SSW-verging extensional meso-structures associated with the negative inversion of the thrust. As shown in the cross section of Figure 12, the thrust has been later offset by the Circeo extensional fault. This extensional fault is part of a system of crustal-scale extensional faults recognized in the seismic line of Figure 3a. Such faults dissect Messinian evaporites and thus started during the Early Pliocene, consistently with the interpretation of other authors in this area (e.g., Conti et al., 2017). The age of calcite fibers associated with S-like-C/C′ fabrics in the Circeo fault zone indicates Langhian to Serravallian (15.6 ± 1.9 Ma to 12.7 ± 2.0 Ma; Figure 11) age for thrusting. The extensional mesostructures collected along the Circeo thrust at the TF site provide a similar age but with a large error (15.8 ± 6.7 Ma and 13.6 ± 7.2 Ma; Figure 11). Given that, at the mesoscale, extensional mesostructures systematically postdates the contractional mesostructures in the TF site (Figures 7c and 7d), we exclude that the shift from compression to extension was a cyclic process. Consequently, we exclude that the switch from compression to extension relates to transient periods of extension induced by earthquake stress changes (e.g., Dielforder et al., 2015). Under the assumption that SSW-directed extension postdated NNE-directed compression, the interval for the onset of SSW-directed shearing along the Circeo thrust must be limited only to its post-compressional portion, that is, the range between ~14.7 Ma (oldest possible age for end of compression = 12.7 + 2.0 Ma) and 9.1 Ma (youngest possible age for extensional reactivation = 15.8–6.7 Ma). This interval is older than Tortonian extension at the Zannone Island with U-Pb ages of 7.7 and 7.2 Ma (Curzi, Billi, et al., 2020), the Plio-Pleistocene extension in the Formia Plain constrained with biostratigraphic criteria (Tavani, Cardello, et al., 2021), and predates the Early Pliocene major extensional faults offshore Circeo. Pliocene back arc extension, the last event that shaped the Circeo promontory, was responsible for the development of the major normal faults seen in the offshore seismic line (Figure 3a) and of the Circeo extensional fault that bound the Circeo promontory to the SW and whose damage zone is exposed at the BPR site (Figure 9). We propose that the Pliocene Circeo extensional fault partly reused the steepened ramp of the Circeo thrust (Figure 12). It is worth noting that the main extensional pulse in the Circeo area started during the Pliocene, but the negative inversion of the thrust largely predated it. We discard the hypothesis that such a negative inversion has occurred in a very early stage of back-arc extension. Indeed, during the 14.7–9.1 Ma time interval, the major thrusts ahead of the Circeo (i.e., the Volsci Range and Mt. Massico thrusts), were not yet active and these areas were still in a foredeep environment, meaning that the Circeo area still represented the compressional front of the belt.

As shown in Figures 12 and 13, we interpret the extensional SSW-directed shearing along the Circeo thrust (Figures 7c and 7d) to be related to the activation of the underlying Mara thrust and associated doming and the stretching in the upper thrust sheet (e.g., Suppe, 1983). This process was likely enhanced by gravitational sliding of the hanging wall along the steepened ramp of the Circeo thrust, as proposed for some structures of the external portion of the Apennines (e.g., Ghisetti & Vezzani, 2000; Patacca et al., 2008). We speculate that the 14.7–9.1 Ma interval likely corresponds to the period of activity of the Mara thrust underneath the Circeo thrust. The high TΔ47 temperatures of extensional slickenfibers indicates a partial synchronous activity of the Circeo and Mara

thrusts, that is, the Mara thrust would have started already during the late stage of activity of the Circeo thrust, when the tectonic burial of the Circeo Flysch was still increasing. This tectonic scenario corresponds to the thermal modeling scenario 2 in the thermal modeling section, in which the Circeo Flysch reached maximum burial conditions and temperatures of nearly 120°C at 12.7 Ma (Figure 14), consistent with TΔ47 temperature of extensional slickenfibers.

5.4. Regional Framework

In addition to the already known Circeo thrust (Accordi, 1966), here we have documented the existence of the previously unrecognized buried Mara thrust, which was responsible for the folding of the Circeo thrust in Miocene time. We connect the Mara thrust with the thrust found at the bottom of the Mara-1 well (Figure 2b), which puts in contact the base of the Lower Jurassic Calcare Massiccio Fm. with Paleocene-Eocene slope/basinal carbonates. This thrust found in the Mara-1 well has one of the largest stratigraphic separations among the thrusts of the central Apennines (more than 3 km), however, it cannot be followed along strike (i.e., NW of the Mara well, in the Volsci Range). The first thrust that can be regionally connected with it, indeed, is the Mara thrust below the Circeo promontory (Figure 12), whose initiation has been constrained to ∼14.7–9.1 Ma interval. The Mara thrust would thus be roughly WNW-ESE striking, slightly oblique to the main NW-SE trend of thrusts in the Apennines, and would possibly retrace the boundary between shallow-water carbonates of the Latium-Abruzzi carbonate platform (exposed in the Volsci Range and at Mt. Massico) and the pelagic basin carbonates of the Circeo pelagic basin (exposed at the Circeo promontory and found in the Mara-1 well; Figure 2a). The overlap between the Mara thrust and the northern boundary of the Circeo pelagic basin corroborates our idea that the Mara thrust could have formed by partial reuse of Jurassic normal faults (Figure 12). Our balanced cross-section indicates that the Circeo and Mara thrusts have accommodated about 10 km of shortening. This is consistent with the amount of shortening commonly proposed in thin-skinned reconstructions for Latium coastal area (e.g., Ghisetti et al., 1993; Mostardini & Merlini, 1986).

We have documented for the first time the occurrence of crustal scale N-S and E-W striking Jurassic faults in the Circeo promontory. These faults have a cumulative displacement in the order of 1 km and are evidenced by paleoescarpments marked by unconformable contacts between the syn- and pre-rift sequences. Also, although with uncertainties and extrapolation from the neighboring Umbria-Marche basin, here we have first provided a plausible thickness of the stratigraphic succession of the Circeo basin, which honors all the available information, including results from our burial and thermal modeling.

Lastly, the interpretation of the offshore seismic line in Figure 3a is consistent with the occurrence of syn-orogenic deposits in the footwall of the Zannone thrust, as proposed by Curzi, Billi, et al. (2020). By removing the shortening associated with the Circeo thrust, we obtain a distance of ca. 30 km between the exposures of the Zannone and Circeo flysch (restored section in Figure 12). This strongly suggests that the two exposures were part of the same syn-orogenic basin. We note, however, that these flysch exposures, and the nearby flysch exposed in the Formia plain-Mt. Massico area, have different clasts composition deriving from different sources: (a) the Zannone flysch is quartz-rich and includes Cretaceous detrital material (Curzi, Billi, et al., 2020); (b) the Circeo flysch includes calcarenitic levels and Lower Miocene resedimented fossils; (c) the conglomerate interfingered with the Mt. Massico flysch has clasts of Mesozoic carbonates and of granite of unknown age (Tavani, Cardello, et al., 2021). These observations suggest that parts of the syn-orogenic units were deposited in a wedge-top setting, where small-sized and compartmentalized basins were filled by sediments sourced by areas that were exposing rocks of different ages, down to the crystalline basement.

5.5. The Orogen Evolution

In the Apennines the eastward retreat of the slab was concurrent with the eastward migration of thrusting and back-arc extension (e.g., Carminati et al., 2012; Doglioni, 1991; Faccenna et al., 2004, 2014). Here, we use our new data to improve the quantification of the time link between slab retreat, compression, and extension within the central Apennines belt. In Figure 15 we integrated our new data with the ages of thrusts and extensional basins in the central Apennines (e.g., Cavinato & De Celles, 1999; Curzi, Billi, et al., 2020 and references therein) and with the age of the base of the foredeep infill in the same area, which is the best available proxy for the age of the forebulge in the central Apennines (Sabbatino et al., 2021 and references therein). The speed

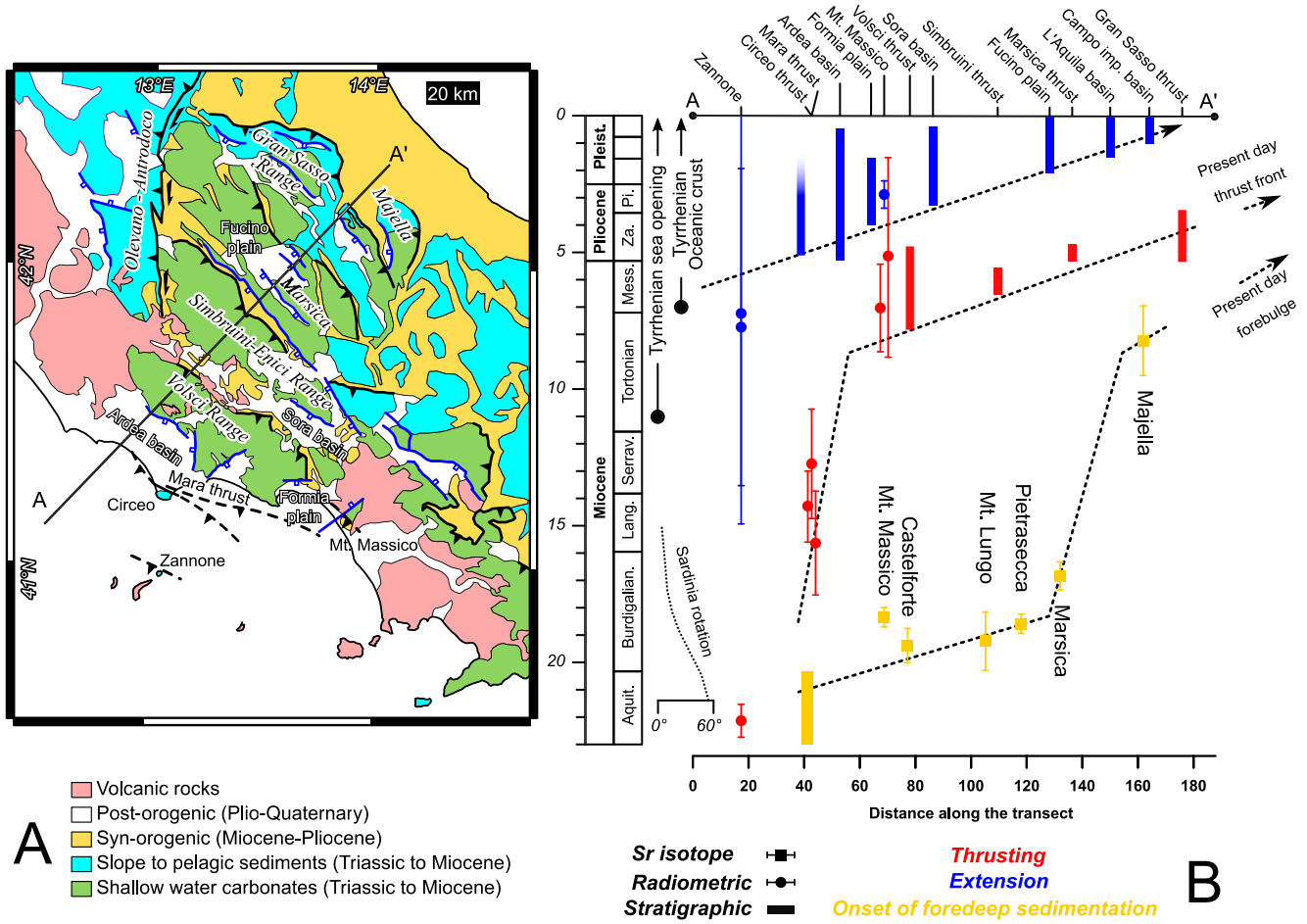

Figure 15. (a) Simplified geological map of the central Apennines. (b) Time-distance transect of extensional and compressional structures, and forebulge/foredeep deposits. The present day thrust front and forebulge, both located >100 km to the NE of the edge of the transect, are taken from Scrocca et al. (2007). Trace of the transect is in (a). The gray stripped lines qualitatively indicate the onset of forebulging, thrusting, and extensional faulting. Data compilation: "Sr isotope" refers to the Strontium isotope dating of the base of the foredeep infill (data from Sabbatino et al. (2021)); "Radiometric" refers to K-Ar dating of clay-rich fault gouge and U-Pb dating of calcite slickenfibers along major thrusts and normal faults (data from Smeraglia et al. (2019) and Curzi, Billi, et al. (2020)); "Stratigraphic" refers to biostratigraphic dating of the base of foredeep infill, piggy back basins, and extensional basins (data from Cavinato and De Celles (1999) and Curzi, Billi, et al. (2020)). Data for the Circeo thrust refer to the three U-Pb ages of compressional slickenfibers. See text for details.

of forebulge migration is taken as a proxy for the velocity of slab retreat. In Figure 15b we projected age data onto a NE-SW oriented transect, whose trace is indicated in Figure 15a. The opening of the Tyrrhenian basin (Faccenna et al., 2004; Sartori et al., 2001), the age of its oceanic crust (Kastens & Mascle, 1990; Savelli & Ligi, 2017), and the opening of the Liguro–Provençal Basin, indicated by the rotation of Sardinia with respect to Europe (Gattacceca et al., 2007), are also reported in the figure. For the sake of simplicity, we did not remove the shortening associated with thrusting. The amount of displacement of all the major thrusts of the central Apennines, excluding the Zannone thrust, is in the order of a few tens of km (e.g., Ghisetti et al., 1993; Mostardini & Merlini, 1986). Removing the displacement of all the thrusts in Figure 15b would simply stretch horizontally (albeit slightly heterogeneously) the thrust front and forebulge distributions, without significantly altering the major steps described below. On the other hand, the removal of the thrust displacement would introduce a bias depending on the model chosen to remove the displacement of the thrusts.

From the Messinian to the present-day, the onset of back-arc extension has constantly migrated toward the foreland (NE), with an average velocity of about 3 cm/yr. In the same period, the onset of thrusting in the frontal structures migrated toward the foreland from the Volsci range-Mt. Massico to the Gran Sasso range, and further NE toward the present day thrust front in the Adriatic Sea (Scrocca et al., 2007), with a constant velocity of ~3 cm/yr, comparable to that of the extensional front. Eventual slab break off processes, proposed to have

occurred in the central Apennines during Late Pliocene time (e.g., Faccenna et al., 2014; Fellin et al., 2022; Wortel & Spakman, 2000), had no significant impact on the foreland-ward migration rate of compressional and extensional fronts. By connecting the age of the base of the syn-orogenic unit of the Majella Mt. (Sabbatino et al., 2021) and the present day forebulge in the Adriatic Sea, a migration rate of 1.7 cm/yr for the forebulge can be calculated. This means that in the central Apennines, since the opening of the Tyrrhenian back arc basin, the forebulge, the thrust front, and the back-arc extension front have all migrated at comparable velocities. Over the past 8 Ma, the distance between the forebulge and the thrust front and between the thrust front and the back-arc extension front have consistently remained at approximately 100 and 70 km, respectively. There is no evidence of back-arc extension older than 8 Ma in the study area. The foreland-ward migration of the thrust front and the forebulge is characterized by slow rates between 18 and 10 Ma, and the distance between the forebulge and the thrust front between 18 and 10 Ma was nearly 100 km. This interval stretches from the final stage of the opening of the Liguro–Provençal back-arc basin (indicated by rotation of Sardinia in Figure 15; e.g., Gattacceca et al., 2007) to the onset of extension in the Tyrrhenian basin (Faccenna et al., 2004; Mattei et al., 2002; Sartori et al., 2001). In this period of quiescence/strong reduction of back-arc extension and deceleration of trench retreat, the foreland-ward migration of the forebulge decelerated to attain values of about 0.3 cm/yr. A similar velocity decrease can be inferred for the thrust front migration in the same period. Before 18 Ma, during the main phase of opening of the Liguro-Provençal back-arc basin, the forebulge migration velocity is again characterized by velocities of about 3 cm/yr. The reconstruction of the pre 20 Ma thrust front migration is challenging, due to the occurrence of only one thrust of unknown displacement (i.e., the Zannone thrust). This thrust, affecting the distal portion of the Circeo pelagic basin, could be a remnant of the typical basal décollement developing in the distal portions of rifted margins during soft collision (Tavani, Granado, et al., 2021). Those kinds of thrusts easily attain displacements in the order of hundreds of km, such as for the High Zagros Fault in the Zagros Belt (e.g., Vergés et al., 2011), the Hawasina thrust in the Oman Mts. (Béchennec et al., 1988), the Tili thrust in Taiwan (Brown et al., 2012), or the Liguride complex of the Apennines (e.g., Tavani, Granado, et al., 2021). The uncertainty about the displacement of the Zannone thrust, prevents any inference on thrust front propagation before 20 Ma.

In summary, the combined analysis of the forebulge, thrust front and back-extension migration curves individuates three different periods, overlapping the opening of the back-arc basins. During the opening of the Liguro–Provençal and Tyrrhenian back-arc basins, the forelandward migration of the forebulge was faster than recorded in the intervening quiescent period, when back-arc extension and E-retreat of the subduction zone were reduced (e.g., Faccenna et al., 2004). We also observe that during the opening of the Tyrrhenian back arc-basin, the thrust front migration accelerated with respect to the previous period, that is, between the opening of the two back arc basins when the thrust front forelandward propagation rate was drastically reduced and only the Circeo and Mara thrusts formed. Little can be said instead about the pre 20 Ma evolution, because coeval structures are buried beneath the Tyrrhenian Sea.

6. Conclusions

We show that the Circeo thrust developed as a thin-skinned structure during Langhian-Serravallian time. Extensional reactivation of the thrust is dated at the Middle Miocene and resulted from the activation of the underlying Mara thrust, which folded the Circeo thrust and steepened its ramp, triggering its negative inversion. The thrust stack was later affected by Pliocene extensional tectonics associated with the opening of the Tyrrhenian back-arc basin.

Integration of our results with the age of the thrusts, extensional basins, and forebulge/foredeep deposits of the central Apennines reveals a link between trench retreat and the kinematics of thrust wedge and back-arc basins. The Circeo thrust system developed during a period of slow/quiescent trench retreat, after the opening of the Liguro-Provençal basin and before the opening of the Tyrrhenian back-arc basin. Similarly, in this period, the forebulge and the thrust front were migrating toward the foreland synchronously at slow velocity. These velocities drastically increased at about 8 Ma, during the opening of the Tyrrhenian back-arc basin. Since then, in the central Apennines, the forebulge, the thrust front, and the back-arc extension front formed three parallel domains that migrated forelandward at a nearly constant velocity of 3 cm/yr.

Our work demonstrates with unprecedented resolution the link between the evolution of the central Apennines thrust belt and of the subsequent post-orogenic extension and velocities of slab retreat.

Data Availability Statement

Details on the data used to build the stratigraphic succession of the Circeo basin are provided in Supporting Information S1. Bedding and fault data collected in the Circeo promontory are archived in Tavani (2022b) available as data in Earthchem via https://doi.org/10.26022/IEDA/112695. Data for C, O, and Clumped Isotopes Analysis are archived in Tavani (2022a) available as data in Earthchem via https://doi.org/10.26022/IEDA/112696. Data for U.Pb dating are archived in Tavani (2022c) and Tavani and Kylander-Clark (2023) available as data in Earthchem via https://doi.org/10.26022/IEDA/112697 and https://doi.org/10.26022/IEDA/112904. All the data are available with open access conditions and license by CC BY 4.0.

Acknowledgments
Armin Dielforder, Nicolas Beaudoin, and an anonymous reviewer, as well as the Editor Laurent Jolivet, are gratefully acknowledged for thoughtful and constructive reviews. We thank Isabella Raffi (University of Chieti) for the help with Nannoplankton analysis and Alessandro Iannace (University of Naples) for help in the field. Madalina Jaggi (ETH) and Stewart Bishop (ETH) are warmly thanked support with isotope analyses. This work has been funded by the Progetti di Ateneo Sapienza L. Aldega and E. Carminati.

References

Accordi, B. (1966). La componente traslativa nella tettonica dell'Appennino laziale-abruzzese. *Geologica Romana*, *5*, 355–406.
Acocella, V., & Funiciello, R. (2006). Transverse systems along the extensional Tyrrhenian margin of central Italy and their influence on volcanism. *Tectonics*, *25*(2), TC2003. https://doi.org/10.1029/2005TC001845
Aldega, L., Carminati, E., Scharf, A., & Mattern, F. (2021). Thermal maturity of the Hawasina units and origin of the Batinah Mélange (Oman Mountains): Insights from clay minerals. *Marine and Petroleum Geology*, *133*, 105316. https://doi.org/10.1016/j.marpetgeo.2021.105316
Anderson, N. T., Kelson, J. R., Kele, S., Daëron, M., Bonifacie, M., Horita, J., et al. (2021). A unified clumped isotope thermometer calibration (0.5–1,100°C) using carbonate-based standardization. *Geophysical Research Letters*, *48*(7), e2020GL092069. https://doi.org/10.1029/2020GL092069
Ault, A. K., Gautheron, C., & King, G. E. (2019). Innovations in (U–Th)/He, fission track, and trapped charge thermochronometry with applications to earthquakes, weathering, surface-mantle connections, and the growth and decay of mountains. *Tectonics*, *38*(11), 3705–3739. https://doi.org/10.1029/2018TC005312
Balestra, M., Corrado, S., Aldega, L., Gasparo Morticelli, M., Sulli, A., Rudkiewicz, J.-L., & Sassi, W. (2019). Thermal and structural modeling of the Scillato wedge-top basin source-to-sink system: Insights into the Sicilian fold-and-thrust belt evolution (Italy). *Geological Society of American Bulletin*, *131*(11–12), 1763–1782. https://doi.org/10.1130/B35078.1
Barchi, M. (2010). The Neogene–Quaternary evolution of the Northern Apennines: Crustal structure, style of deformation and seismicity. *Journal of the Virtual Explorer*, *36*(10). https://doi.org/10.3809/jvirtex.2010.00220
Beaudoin, N., Bellahsen, N., Lacombe, O., Emmanuel, L., & Pironon, J. (2014). Crustal-scale fluid flow during the tectonic evolution of the Bighorn Basin (Wyoming, USA). *Basin Research*, *26*(3), 403–435. https://doi.org/10.1111/bre.12032
Beaudoin, N., Huyghe, D., Bellahsen, N., Lacombe, O., Emmanuel, L., Mouthereau, F., & Ouanhnon, L. (2015). Fluid systems and fracture development during syn-depositional fold growth: An example from the Pico del Aguila anticline, Sierras Exteriores, southern Pyrenees, Spain. *Journal of Structural Geology*, *70*, 23–38. https://doi.org/10.1016/j.jsg.2014.11.003
Beaudoin, N., Leprêtre, R., Bellahsen, N., Lacombe, O., Amrouch, K., Callot, J. P., et al. (2012). Structural and microstructural evolution of the Rattlesnake Mountain Anticline (Wyoming, USA): New insights into the Sevier and Laramide orogenic stress build-up in the Bighorn Basin. *Tectonophysics*, *576*, 20–45. https://doi.org/10.1016/j.tecto.2012.03.036
Beaudoin, N. E., Labeur, A., Lacombe, O., Koehn, D., Billi, A., Hoareau, G., et al. (2020). Regional-scale paleofluid system across the Tuscan Nappe–Umbria–Marche Apennine Ridge (northern Apennines) as revealed by mesostructural and isotopic analyses of stylolite–vein networks. *Solid Earth*, *11*(4), 1617–1641. https://doi.org/10.5194/se-11-1617-2020
Béchennec, F., Le Métour, J., Rabu, D., Villey, M., & Beurrier, M. (1988). The Hawasina Basin: A fragment of a starved passive continental margin, thrust over the Arabian Platform during obduction of the Sumail Nappe. *Tectonophysics*, *151*(1–4), 323–343. https://doi.org/10.1016/0040-1951(88)90251-X
Bernasconi, S. M., Daëron, M., Bergmann, K. D., Bonifacie, M., Meckler, A. N., Affek, H. P., et al. (2021). InterCarb: A community effort to improve interlaboratory standardization of the carbonate clumped isotope thermometer using carbonate standards. *Geochemistry, Geophysics, Geosystems*, *22*(5), e2020GC009588. https://doi.org/10.1029/2020GC009588
Bernoulli, D., Kälin, O., & Patacca, E. (1979). A sunken continental margin of the Mesozoic Tethys: The northern and central Apennines. In B. Beaudoin & B. H. Purser (Eds.), *Symposium: "Sédimentation Jurassique W européen"* (Vol. 1, pp. 197–210). Publication Spécial Association Sédimentologique Française.
Beyssac, O., Goffé, B., Chopin, C., & Rouzaud, J. (2002). Raman spectra of carbonaceous material in metasediments: A new geothermometer. *Journal of Metamorphic Geology*, *20*(9), 859–871. https://doi.org/10.1046/j.1525-1314.2002.00408.x
Billi, A., Tiberti, M. M., Cavinato, G. P., Cosentino, D., Di Luzio, E., Keller, J. V. A., et al. (2006). First results from the CROP-11 deep seismic profile, central Apennines, Italy: Evidence of mid-crustal folding. *Journal of the Geological Society*, *163*(4), 583–586. https://doi.org/10.1144/0016-764920-002
Bown, P. R., & Young, J. R. (1998). Calcareous Nannofossil Biostratigraphy. In *Calcareous Nannofossil Biostratigraphy*.
Brown, D., Alvarez-Marron, J., Schimmel, M., Wu, Y.-M., & Camanni, G. (2012). The structure and kinematics of the central Taiwan mountain belt derived from geological and seismicity data. *Tectonics*, *31*(5), TC5013. https://doi.org/10.1029/2012TC003156
Burnham, A. K., & Sweeney, J. J. (1989). A chemical kinetic model of vitrinite maturation and reflectance. *Geochimica et Cosmochimica Acta*, *53*(10), 2649–2657. https://doi.org/10.1016/0016-7037(89)90136-1
Butler, R. W. H. (1992). Hydrocarbon maturation, migration and tectonic loading in the western Alps. *Geological Society of London, Special Publications*, *59*(1), 227–244. https://doi.org/10.1144/GSL.SP.1991.059.01.15
Cardello, G. L. (2006). Rilevamento geologico del Promontorio del Circeo: Analisi di facies ed evoluzione tettono-stratigrafica (Bachelor Thesis). https://doi.org/10.13140/RG.2.1.1580.7204
Cardello, G. L., Vico, G., Consorti, L., Sabbatino, M., Carminati, E., & Doglioni, C. (2021). Constraining the passive to active margin tectonics of the internal central Apennines: Insights from biostratigraphy, structural, and seismic analysis. *Geosciences*, *11*(4), 160. https://doi.org/10.3390/geosciences11040160
Carminati, E., & Doglioni, C. (2012). Alps vs. Apennines: The paradigm of a tectonically asymmetric Earth. *Earth-Science Reviews*, *112*(1–2), 67–96. https://doi.org/10.1016/j.earscirev.2012.02.004
Carminati, E., Lustrino, M., & Doglioni, C. (2012). Geodynamic evolution of the central and western Mediterranean: Tectonics vs. igneous petrology constraints. *Tectonophysics*, *579*, 173–192. https://doi.org/10.1016/j.tecto.2012.01.026

Cassinis, G., Perotti, C., & Santi, G. (2018). Post-Variscan Verrucano-like deposits in Italy, and the onset of the alpine tectono-sedimentary cycle. *Earth-Science Reviews*, *185*, 476–497. https://doi.org/10.1016/j.earscirev.2018.06.021

Castellarin, A., Colacicchi, R., & Praturlon, A. (1978). Fasi distensive, trascorrenze e sovrascorrimenti lungo la "Linea Ancona-Anzio", dal Lias medio al Pliocene. *Geologica Romana*, *17*, 161–189.

Cavinato, G. P., & De Celles, P. D. (1999). Extensional basins in the tectonically bimodal central Apennines fold-thrust belt, Italy: Response to corner flow above a subducting slab in retrograde motion. *Geology*, *27*(10), 955–958. https://doi.org/10.1130/0091-7613(1999)027<0955:EBITTB>2.3.CO;2

Cerchiari, A., Remitti, F., Mittempergher, S., Festa, A., Lugli, F., & Cipriani, A. (2020). Cyclical variations of fluid sources and stress state in a shallow megathrust-zone mélange. *Journal of the Geological Society*, *177*(3), 647–659. https://doi.org/10.1144/jgs2019-072

Chiarabba, C., Jovane, L., & DiStefano, R. (2005). A new view of Italian seismicity using 20 years of instrumental recordings. *Tectonophysics*, *395*(3–4), 251–268. https://doi.org/10.1016/j.tecto.2004.09.013

Cipollari, P., & Cosentino, D. (1995). Miocene unconformities in the Central Apennines: Geodynamic significance and sedimentary basin evolution. *Tectonophysics*, *252*(1–4), 375–389. https://doi.org/10.1016/0040-1951(95)00088-7

Conti, A., Bigi, S., Cuffaro, M., Doglioni, C., Scrocca, D., Muccini, F., et al. (2017). Transfer zones in an oblique back-arc basin setting: Insights from the Latium-Campania segmented margin (Tyrrhenian Sea). *Tectonics*, *36*(1), 78–107. https://doi.org/10.1002/2016TC004198

Cosentino, D., Cipollari, P., Marsili, P., & Scrocca, D. (2010). Geology of the central Apennines: A regional review. *Journal of the Virtual Explorer*, *36*, 1–37. https://doi.org/10.3809/jvirtex.2010.00223

Cruset, D., Cantarero, I., Vergés, J., John, C. M., Muñoz-López, D., & Travé, A. (2018). Changes in fluid regime in syn-orogenic sediments during the growth of the south Pyrenean fold and thrust belt. *Global and Planetary Change*, *171*, 207–224. https://doi.org/10.1016/j.gloplacha.2017.11.001

Cruset, D., Vergés, J., Albert, R., Gerdes, A., Benedicto, A., Cantarero, I., & Travé, A. (2020). Quantifying deformation processes in the SE Pyrenees using U–Pb dating of fracture-filling calcites. *Journal of the Geological Society*, *177*(6), 1186–1196. https://doi.org/10.1144/jgs2020-014

Curzi, M., Aldega, L., Bernasconi, S. M., Berra, F., Billi, A., Boschi, C., et al. (2020). Architecture and evolution of an extensionally-inverted thrust (Mt. Tancia Thrust, Central Apennines): Geological, structural, geochemical, and K–Ar geochronological constraints. *Journal of Structural Geology*, *136*, 104059. https://doi.org/10.1016/j.jsg.2020.104059

Curzi, M., Billi, A., Carminati, E., Rossetti, F., Albert, R., Aldega, L., et al. (2020). Disproving the presence of Paleozoic-Triassic metamorphic rocks on the Island of Zannone (central Italy): Implications for the early stages of the Tyrrhenian-Apennines tectonic evolution. *Tectonics*, *39*(12), e2020TC006296. https://doi.org/10.1029/2020TC006296

Daëron, M., Blamart, D., Peral, M., & Affek, H. P. (2016). Absolute isotopic abundance ratios and the accuracy of Δ47 measurements. *Chemical Geology*, *442*, 83–96. https://doi.org/10.1016/j.chemgeo.2016.08.014

D'Agostino, N., Chamot-Rooke, N., Funiciello, R., Jolivet, L., & Speranza, F. (1998). The role of pre-existing thrust faults and topography on the styles of extension in the Gran Sasso range (central Italy). *Tectonophysics*, *292*(3–4), 229–254. https://doi.org/10.1016/S0040-1951(98)00070-5

Dahlstrom, C. D. A. (1969). Balanced cross sections. *Canadian Journal of Earth Sciences*, *6*(4), 743–757. https://doi.org/10.1139/e69-069

Dielforder, A., Berger, A., & Herwegh, M. (2016). The accretion of foreland basin sediments during early stages of continental collision in the European Alps and similarities to accretionary wedge tectonics. *Tectonics*, *35*(10), 2216–2238. https://doi.org/10.1002/2015TC004101

Dielforder, A., Vollstaedt, H., Vennemann, T., Berger, A., & Herwegh, M. (2015). Linking megathrust earthquakes to brittle deformation in a fossil accretionary complex. *Nature Communications*, *6*(1), 7504. https://doi.org/10.1038/ncomms8504

Di Stefano, S., Bianchi, I., Ciaccio, M. G., Carrara, G., & Kissling, E. (2011). Three-dimensional Moho topography in Italy: New constraints from receiver functions and controlled source seismology. *Geochemistry, Geophysics, Geosystems*, *12*(9), Q09006. https://doi.org/10.1029/2011GC003649

Doglioni, C. (1991). A proposal for the kinematic modelling of W-dipping subductions-possible applications to the Tyrrhenian-Apennines system. *Terra Nova*, *3*(4), 423–434. https://doi.org/10.1111/j.1365-3121.1991.tb00172.x

Ducoux, M., Jolivet, L., Cagnard, F., & Baudin, T. (2021). Basement-cover decoupling during the inversion of a hyperextended basin: Insights from the Eastern Pyrenees. *Tectonics*, *40*(5), e2020TC006512. https://doi.org/10.1029/2020TC006512

Evans, M. A., & Fischer, M. P. (2012). On the distribution of fluids in folds: A review of controlling factors and processes. *Journal of Structural Geology*, *44*, 2–24. https://doi.org/10.1016/j.jsg.2012.08.003

Fabbi, S. (2015). Geology and Jurassic paleogeography of the Mt. Primo-Mt. Castel Santa Maria ridge and neighbouring areas (Northern Apennines, Italy). *Journal of Maps*, *11*(4), 645–663. https://doi.org/10.1080/17445647.2014.956235

Faccenna, C., Becker, T. W., Auer, L., Billi, A., Boschi, L., Brun, J. P., et al. (2014). Mantle dynamics in the Mediterranean. *Reviews of Geophysics*, *52*(3), 283–332. https://doi.org/10.1002/2013RG000444

Faccenna, C., Piromallo, C., Crespo-Blanc, A., Jolivet, L., & Rossetti, F. (2004). Lateral slab deformation and the origin of the western Mediterranean arcs. *Tectonics*, *23*(1), TC1012. https://doi.org/10.1029/2002TC001488

Fellin, M. G., San Jose, M., Faccenna, C., Willett, S. D., Cosentino, D., Lanari, R., et al. (2022). Transition from slab roll-back to slab break-off in the central Apennines, Italy: Constraints from the stratigraphic and thermochronologic record. *Geological Society of American Bulletin*, *134*(7–8), 1916–1930. https://doi.org/10.1130/B36123.1

Fernandez, A., Müller, I. A., Rodríguez-Sanz, L., van Dijk, J., Looser, N., & Bernasconi, S. M. (2017). A reassessment of the precision of carbonate clumped isotope measurements: Implications for calibrations and paleoclimate reconstructions. *Geochemistry, Geophysics, Geosystems*, *18*(12), 4375–4386. https://doi.org/10.1002/2017GC007106

Gattacceca, J., Deino, A., Rizzo, R., Jones, D. S., Henry, B., Beaudoin, B., & Vedeboin, F. (2007). Miocene rotation of Sardinia: New paleomagnetic and geochronological constraints and geodynamic implications. *Earth and Planetary Science Letters*, *258*(3–4), 359–377. https://doi.org/10.1016/j.epsl.2007.02.003

Ghisetti, F., Barchi, M., Bally, A. W., Moretti, I., & Vezzani, L. (1993). Conflicting balanced structural sections across the Central Apennines (Italy): Problems and implications. In *Generation, accumulation and production of Europe's hydrocarbons III* (pp. 219–231). Springer.

Ghisetti, F., & Vezzani, L. (2000). Detachments and normal faulting in the Marche fold-and-thrust belt (central Apennines, Italy): Inferences on fluid migration paths. *Journal of Geodynamics*, *29*(3–5), 345–369. https://doi.org/10.1016/s0264-3707(99)00057-5

Hardebeck, J. L., & Okada, T. (2018). Temporal stress changes caused by earthquakes: A review. *Journal of Geophysical Research: Solid Earth*, *123*(2), 1350–1365. https://doi.org/10.1002/2017JB014617

Henkes, G. A., Passey, B. H., Grossman, E. L., Shenton, B. J., Pérez-Huerta, A., & Yancey, T. E. (2014). Temperature limits for preservation of primary calcite clumped isotope paleotemperatures. *Geochimica et Cosmochimica Acta*, *139*, 362–382. https://doi.org/10.1016/j.gca.2014.04.040

Hillier, S., Màtyàs, J., Matter, A., & Vasseur, G. (1995). Illite/smectite diagenesis and its variable correlation with vitrinite reflectance in the Pannonian Basin. *Clays and Clay Minerals*, *43*(2), 174–183. https://doi.org/10.1346/CCMN.1995.0430204

Hossack, J. R. (1979). The use of balanced cross-sections in the calculation of orogenic contraction: A review. *Journal of the Geological Society*, *136*(6), 705–711. https://doi.org/10.1144/gsjgs.136.6.0705

Jagodzinski, H. (1949). Eindimensionale Fehlordnung in Kristallen und ihr Einfluss auf die Röntgen Interferenzen. *Acta Crystallographica*, *2*(4), 201–207. https://doi.org/10.1107/s0365110x49000552

John, C. M., & Bowen, D. (2016). Community software for challenging isotope analysis: First applications of 'Easotope' to clumped isotopes. *Rapid Communications in Mass Spectrometry*, *30*(21), 2285–2300. https://doi.org/10.1002/rcm.7720

Jolivet, L., Faccenna, C., Goffé, B., Mattei, M., Rossetti, F., Brunet, C., et al. (1998). Midcrustal shear zones in postorogenic extension: Example from the northern Tyrrhenian Sea. *Journal of Geophysical Research*, *103*(B6), 12123–12160. https://doi.org/10.1029/97JB03616

Jolivet, L., Faccenna, C., & Piromallo, C. (2009). From mantle to crust: Stretching the Mediterranean. *Earth and Planetary Science Letters*, *285*(1–2), 198–209. https://doi.org/10.1016/j.epsl.2009.06.017

Jolivet, L., Menant, A., Roche, V., Le Pourhiet, L., Maillard, A., Augier, R., et al. (2021). Transfer zones in Mediterranean back-arc regions and tear faults. *Bulletin de la Societe Geologique de France*, *192*(1), 11. https://doi.org/10.1051/bsgf/2021006

Kastens, K., & Mascle, J. (1990). The geological evolution of the Tyrrhenian Sea: An introduction to the scientific results of ODP Leg 107. In K. Kastens & J. Mascle (Eds.), *Proceedings of the Ocean Drilling Program, Scientific Results* (Vol. 107, pp. 3–26). https://doi.org/10.2973/odp.proc.sr.107.187.1990

Knott, S. D. (1987). The Liguride complex of southern Italy: A Cretaceous to Paleogene accretionary wedge. *Tectonophysics*, *142*(2–4), 217–226. https://doi.org/10.1016/0040-1951(87)90124-7

Koehn, D., & Passchier, C. W. (2000). Shear sense indicators in striped bedding-veins. *Journal of Structural Geology*, *22*(8), 1141–1151. https://doi.org/10.1016/S0191-8141(00)00028-6

Labeur, A., Beaudoin, N. E., Lacombe, O., Emmanuel, L., Petracchini, L., Daëron, M., et al. (2021). Burial-deformation history of folded rocks unraveled by fracture analysis, stylolite paleopiezometry and vein cement geochemistry: A case ctudy in the Cingoli Anticline (Umbria–Marche, Northern Apennines). *Geosciences*, *11*(3), 135. https://doi.org/10.3390/geosciences11030135

Lacombe, O., Amrouch, K., Mouthereau, F., & Dissez, L. (2007). Calcite twinning constraints on late Neogene stress patterns and deformation mechanisms in the active Zagros collision belt. *Geology*, *35*(3), 263–266. https://doi.org/10.1130/G23173A.1

Lacombe, O., & Beaudoin, N. E. (2024). Timing, sequence, duration and rate of deformation in fold-and-thrust belts: A review of traditional approaches and recent advances from absolute dating (K–Ar illite/U–Pb calcite) of brittle structures. *Comptes Rendus Geoscience*, *S2*, 1–28. https://doi.org/10.5802/crgeos.218

Lacombe, O., Beaudoin, N. E., Hoareau, G., Labeur, A., Pecheyran, C., & Callot, J. P. (2021). Dating folding beyond folding, from layer-parallel shortening to fold tightening, using mesostructures: Lessons from the Apennines, Pyrenees, and Rocky Mountains. *Solid Earth*, *12*(10), 2145–2157. https://doi.org/10.5194/se-12-2145-2021

Lucca, A., Storti, F., Balsamo, F., Clemenzi, L., Fondriest, M., Burgess, R., & Di Toro, G. (2019). From submarine to subaerial out-of-sequence thrusting and gravity-driven extensional faulting: Gran Sasso Massif, Central Apennines, Italy. *Tectonics*, *38*(12), 4155–4184. https://doi.org/10.1029/2019TC005783

Marroni, M., Molli, G., Montanini, A., & Tribuzio, R. (1998). The association of continental crust rocks with ophiolites in the Northern Apennines (Italy): Implications for the continent-ocean transition in the Western Tethys. *Tectonophysics*, *292*(1–2), 43–66. https://doi.org/10.1016/S0040-1951(98)00060-2

Mattei, M., Cipollari, P., Cosentino, D., Argentieri, A., Rossetti, F., Speranza, F., et al. (2002). The Miocene tectonic evolution of the Southern Tyrrhenian Sea: Stratigraphy, structural and paleomagnetic data from the on-shore Amantea basin (Calabrian Arc, Italy). *Basin Research*, *14*(2), 147–168. https://doi.org/10.1046/j.1365-2117.2002.00173.x

McClay, K. R. (1992). Glossary of thrust tectonics terms. In K. R. McClay (Ed.), *Thrust tectonics*. Chapman & Hall.

McQuarrie, N., Barnes, J. B., & Ehlers, T. A. (2008). Geometric, kinematic, and erosional history of the central Andean Plateau, Bolivia (15–17°S). *Tectonics*, *27*(3), TC3007. https://doi.org/10.1029/2006TC002054

Meckler, A. N., Ziegler, M., Millán, M. I., Breitenbach, S. F., & Bernasconi, S. M. (2014). Long-term performance of the Kiel carbonate device with a new correction scheme for clumped isotope measurements. *Rapid Communications in Mass Spectrometry*, *28*(15), 1705–1715. https://doi.org/10.1002/rcm.6949

Menardi Noguera, A., & Rea, G. (2000). Deep structure of the Campanian–Lucanian arc (southern Apennine, Italy). *Tectonophysics*, *324*(4), 239–265. https://doi.org/10.1016/S0040-1951(00)00137-2

Meneghini, F., & Moore, J. C. (2007). Deformation and hydrofracture in a subduction thrust at seismogenic depths: The Rodeo Cove thrust zone, Marin Headlands, California. *Geological Society of America Bulletin*, *119*(1–2), 174–183. https://doi.org/10.1130/B25807.1

Mirabella, F., Barchi, M., Lupattelli, A., Stucchi, E., & Ciaccio, M. G. (2008). Insights on the seismogenic layer thickness from the upper crust structure of the Umbria-Marche Apennines (central Italy). *Tectonics*, *27*(1), TC1010. https://doi.org/10.1029/2007TC002134

Molli, G. (2008). Northern Apennine–Corsica orogenic system: An updated overview. *Geological Society of London, Special Publications*, *298*(1), 413–442. https://doi.org/10.1144/SP298.19

Montone, P., & Mariucci, M. T. (2016). The new release of the Italian contemporary stress map. *Geophysical Journal International*, *205*(3), 1525–1531. https://doi.org/10.1093/gji/ggw100

Moore, D. M., & Reynolds, R. C., Jr. (1997). *X-Ray Diffraction and the identification and analysis of clay minerals* (p. 378). Oxford University Press.

Mostardini, F., & Merlini, S. (1986). Appennino centro-meridionale. Sezioni geologiche e proposta di modello strutturale. *Memorie Società Geologica Italiana*, *35*, 177–202.

Müller, I. A., Fernandez, A., Radke, J., Van Dijk, J., Bowen, D., Schwieters, J., & Bernasconi, S. M. (2017). Carbonate clumped isotope analyses with the long-integration dual-inlet (LIDI) workflow: Scratching at the lower sample weight boundaries. *Rapid Communications in Mass Spectrometry*, *31*(12), 1057–1066. https://doi.org/10.1002/rcm.7878

Nuriel, P., Weinberger, R., Kylander-Clark, A. R. C., Hacker, B. R., & Craddock, J. P. (2017). The onset of the Dead Sea transform based on calcite age-strain analyses. *Geology*, *45*(7), 587–590. https://doi.org/10.1130/G38903.1

O'Neil, J. R., Clayton, R. N., & Mayeda, T. K. (1969). Oxygen isotope fractionation in divalent metal carbonates. *The Journal of Chemical Physics*, *51*(12), 5547–5558. https://doi.org/10.1063/1.1671982

Pace, P., Pasqui, V., Tavarnelli, E., & Calamita, F. (2017). Foreland-directed gravitational collapse along curved thrust fronts: Insights from a minor thrust-related shear zone in the Umbria–Marche belt, central-northern Italy. *Geological Magazine*, *154*(2), 381–392. https://doi.org/10.1017/S0016756816000200

Pantosti, D., Salvini, F., & Velona, M. (1986). Assetto geologico strutturale del promontorio del Circeo (Italia centrale). *Mem Soc Geol Ital*, *35*, 611–621.

Patacca, E., Scandone, P., Di Luzio, E., Cavinato, G. P., & Parotto, M. (2008). Structural architecture of the central Apennines: Interpretation of the CROP 11 seismic profile from the Adriatic coast to the orographic divide. *Tectonics*, *27*(3), TC3006. https://doi.org/10.1029/2005TC001917

Pierantoni, P., Deiana, G., & Galdenzi, S. (2013). Stratigraphic and structural features of the Sibillini mountains (Umbria-Marche Apennines, Italy). *Italian Journal of Geosciences*, *132*(3), 497–520. https://doi.org/10.3301/IJG.2013.08

Rovida, A., Mario, L., Romano, C., Lolli, B., & Gasperini, P. (2020). The Italian earthquake catalogue CPTI15. *Bulletin of Earthquake Engineering*, *18*(7), 2953–2984. https://doi.org/10.1007/s10518-020-00818-y

Sabbatino, M., Tavani, S., Vitale, S., Ogata, K., Corradetti, A., Consorti, L., et al. (2021). Forebulge migration in the foreland basin system of the central-southern Apennine fold-thrust belt (Italy): New high-resolution Sr-isotope dating constraints. *Basin Research*, *33*(5), 2817–2836. https://doi.org/10.1111/bre.12587

Santantonio, M., & Carminati, E. (2011). Jurassic rifting evolution of the Apennines and Southern Alps (Italy): Parallels and differences. *GSA Bulletin*, *123*(3–4), 468–484. https://doi.org/10.1130/B30104.1

Sartori, R., Carrara, G., Torelli, L., & Zitellini, N. (2001). Neogene evolution of the southwestern Tyrrhenian Sea (Sardinia Basin and western Bathyal Plain). *Marine Geology*, *175*(1–4), 47–66. https://doi.org/10.1016/S0025-3227(01)00116-5

Sartori, R., Torelli, L., Zitellini, N., Carrara, G., Magaldi, M., & Mussoni, P. (2004). Crustal features along a W–E Tyrrhenian transect from Sardinia to Campania margins (Central Mediterranean). *Tectonophysics*, *383*(3–4), 171–192. https://doi.org/10.1016/j.tecto.2004.02.008

Savelli, C., & Ligi, M. (2017). An updated reconstruction of basaltic crust emplacement in Tyrrhenian Sea, Italy. *Scientific Reports*, *7*(1), 1–12. https://doi.org/10.1038/s41598-017-17625-2

Schito, A., Romano, C., Corrado, S., Grigo, D., & Poe, B. (2017). Diagenetic thermal evolution of organic matter by Raman spectroscopy. *Organic Geochemistry*, *106*, 57–67. https://doi.org/10.1016/j.orggeochem.2016.12.006

Schmid, T. W., & Bernasconi, S. M. (2010). An automated method for clumped-isotope measurements on small carbonate samples. *Rapid Communications in Mass Spectrometry*, *24*(14), 1955–1963. https://doi.org/10.1002/rcm.4598

Sclater, J. G., & Christie, P. A. F. (1980). Continental stretching: An explanation of post–Mid Cretaceous subsidence on the central North Sea Basin. *Journal of Geophysical Research*, *85*(B7), 3711–3739. https://doi.org/10.1029/jb085ib07p03711

Scrocca, D., Carminati, E., Doglioni, C., & Marcantoni, D. (2007). Slab retreat and active shortening along the central-northern Apennines. In *Thrust belts and foreland basins* (pp. 471–487). Springer.

Sharp, Z. (2007). *Principles of Stable isotope Geochemistry* (p. 360). Prentice Hall.

Smeraglia, L., Aldega, L., Billi, A., Carminati, E., Di Fiore, F., Gerdes, A., et al. (2019). Development of an intrawedge tectonic mélange by out-of-sequence thrusting, buttressing, and intraformational rheological contrast, Mt. Massico ridge, Apennines, Italy. *Tectonics*, *38*(4), 1223–1249. https://doi.org/10.1029/2018TC005243

Stolper, D. A., & Eiler, J. M. (2015). The kinetics of solid-state isotope-exchange reactions for clumped isotopes: A study of inorganic calcites and apatites from natural and experimental samples. *American Journal of Science*, *315*(5), 363–411. https://doi.org/10.2475/05.2015.01

Storti, F. (1995). Tectonics of the Punta Bianca promontory: Insights for the evolution of the Northern Apennines-Northern Tyrrhenian Sea basin. *Tectonics*, *14*(4), 832–847. https://doi.org/10.1029/95tc01203

Storti, F., Balsamo, F., Mozafari, M., Koopman, A., Swennen, R., & Taberner, C. (2018). Syn-contractional overprinting between extension and shortening along the Montagna dei Fiori Fault during Plio-Pleistocene antiformal stacking at the Central Apennines thrust wedge toe. *Tectonics*, *37*(10), 3690–3720. https://doi.org/10.1029/2018TC005072

Suppe, J. (1983). Geometry and kinematics of fault-bend folding. *American Journal of Science*, *283*(7), 684–721. https://doi.org/10.2475/ajs.283.7.684

Sweeney, J. J., & Burnham, A. K. (1990). Evaluation of a simple model of vitrinite reflectance based on chemical kinetics. *The American Association of Petroleum Geologists Bulletin*, *74*, 1559–1570.

Tari, G., Connors, C., Flinch, J., Granath, J., Pace, P., Sobornov, K., & Soto, J. I. (2023). Negative structural inversion: An overview. *Marine and Petroleum Geology*, *152*, 106223. https://doi.org/10.1016/j.marpetgeo.2023.106223

Tavani, S. (2022a). C, O, and Clumped Isotopes Analysis From Circeo (Italy), Version 1.0 [Dataset]. Interdisciplinary Earth Data Alliance (IEDA). https://doi.org/10.26022/IEDA/112696

Tavani, S. (2022b). Mesostructural data collected in the Circeo promontory (Italy), Version 1.0 [Dataset]. Interdisciplinary Earth Data Alliance (IEDA). https://doi.org/10.26022/IEDA/112695

Tavani, S. (2022c). U-Pb dating of calcite mineralizations in the Circeo Promontory (Italy), Version 1.0 [Dataset]. Interdisciplinary Earth Data Alliance (IEDA). https://doi.org/10.26022/IEDA/112697

Tavani, S., Cardello, G. L., Vignaroli, G., Balsamo, F., Parente, M., Sabbatino, M., et al. (2021). Segmentation of the Apenninic Margin of the Tyrrhenian Back-Arc Basin Forced by the Subduction of an Inherited Transform System. *Tectonics*, *40*(9), e2021TC006770. https://doi.org/10.1029/2021TC006770

Tavani, S., Granado, P., Corradetti, A., Camanni, G., Vignaroli, G., Manatschal, G., et al. (2021). Rift inheritance controls the switch from thin-to thick-skinned thrusting and basal décollement re-localization at the subduction-to-collision transition. *GSA Bulletin*, *133*(9–10), 2157–2170. https://doi.org/10.1130/B35800.1

Tavani, S., & Kylander-Clark, A. (2023). U-Pb dating of calcite mineralizations in the Circeo Promontory (Italy). Part II, Version 1.0 [Dataset]. Interdisciplinary Earth Data Alliance (IEDA). https://doi.org/10.26022/IEDA/112904

Tavani, S., Mencos, J., Bausà, J., & Muñoz, J. A. (2011). The fracture pattern of the Sant Corneli Bóixols oblique inversion anticline (Spanish Pyrenees). *Journal of Structural Geology*, *33*(11), 1662–1680. https://doi.org/10.1016/j.jsg.2011.08.007

Tavani, S., Storti, F., Bausa, J., & Munoz, J. A. (2012). Late thrusting extensional collapse at the mountain front of the northern Apennines (Italy). *Tectonics*, *31*(4), TC4019. https://doi.org/10.1029/2011TC003059

Uysal, I. T., Mutlu, H., Altunel, E., Karabacak, V., & Golding, S. D. (2006). Clay mineralogical and isotopic (K–Ar, $\delta^{18}O$, δD) constraints on the evolution of the North Anatolian Fault Zone, Turkey. *Earth and Planetary Science Letters*, *243*(1–2), 181–194. https://doi.org/10.1016/j.epsl.2005.12.025

Vai, G. B. (2001). Basement and early (pre-Alpine) history. In *Anatomy of an orogen: The Apennines and adjacent Mediterranean basins* (pp. 121–150). Springer. https://doi.org/10.1007/978-94-015-9829-3_10

Vergés, J., Saura, E., Casciello, E., Fernàndez, M., Villaseñor, A., Jiménez-Munt, I., & García-Castelcarlanos, D. (2011). Crustal-scale cross-sections across the NW Zagros belt: Implications for the Arabian margin reconstruction. *Geological Magazine*, *148*(5–6), 739–761. https://doi.org/10.1017/S0016756811000331

Volpe, G., Pozzi, G., Carminati, E., Barchi, M. R., Scuderi, M. M., Tinti, E., et al. (2022). Frictional controls on the seismogenic zone: Insights from the Apenninic basement, Central Italy. *Earth and Planetary Science Letters*, *583*, 117444. https://doi.org/10.1016/j.epsl.2022.117444

Wang, Y., Zwingmann, H., Zhou, L., Lo, C. H., Viola, G., & Hao, J. (2016). Direct dating of folding events by $^{40}Ar/^{39}Ar$ analysis of synkinematic muscovite from flexural-slip planes. *Journal of Structural Geology*, *83*, 46–59. https://doi.org/10.1016/j.jsg.2015.12.003

Wilson, J. T. (1966). Did the Atlantic close and then re-open? *Nature*, *211*(5050), 676–681. https://doi.org/10.1038/211676a0

Wortel, M. J. R., & Spakman, W. (2000). Subduction and slab detachment in the Mediterranean- Carpathian region. *Science*, *290*(5498), 1910–1917. https://doi.org/10.1126/science.290.5498.1910

Zappaterra, E. (1994). Source-rock distribution model of the Periadriatic region. *AAPG Bulletin*, *78*(3), 333–354. https://doi.org/10.1306/bdff90a0-1718-11d7-8645000102c1865d

References From the Supporting Information

Anelli, L., Gorza, M., Pieri, M., & Riva, M. (1994). Subsurface well data in the northern Apennines (Italy). *Memorie della Societa Geologica Italiana*, *48*, 461–471.

Bally, A. W., Burbi, L., Cooper, C., & Ghelardoni, R. (1986). Balanced cross-sections and seismic reflection profiles across the central Apennines. *Memorie della Societa Geologica Italiana*, *35*, 257–310.

Di Francesco, L., Fabbi, S., Santantonio, M., Bigi, S., & Poblet, J. (2010). Contribution of different kinematic models and a complex Jurassic stratigraphy in the construction of a forward model for the Montagna dei Fiori fault-related fold (Central Apennines, Italy). *Geological Journal*, *45*(5–6), 489–505. https://doi.org/10.1002/gj.1191